



**Zeolite-templated carbons - Three-dimensional microporous
graphene frameworks**

Journal:	<i>ChemComm</i>
Manuscript ID	CC-FEA-03-2018-001932.R1
Article Type:	Feature Article

SCHOLARONE™
Manuscripts

Zeolite-templated carbons - Three-dimensional microporous graphene frameworks

Received 00th January 20xx,
Accepted 00th January 20xx

H. Nishihara* and T. Kyotani

DOI: 10.1039/x0xx00000x

www.rsc.org/

Zeolite-templated carbons (ZTCs) are ordered microporous carbons synthesized by using zeolite as a sacrificial template. Unlike well-known ordered mesoporous carbons obtained by using mesoporous silica templates, ZTCs are consisting of curved and single-layer graphene frameworks, thereby affording uniform micropore size (ca. 1.2 nm), developed microporosity ($\sim 1.7 \text{ cm}^3 \text{ g}^{-1}$), very high surface areas ($\sim 4000 \text{ m}^2 \text{ g}^{-1}$), good compatibility with chemical modification, and remarkable softness/elasticity. Thus, ZTCs have been applied to many applications such as hydrogen storage, methane storage, CO_2 capture, liquid-phase adsorption, catalysts, electrochemical capacitors, batteries, and fuel cells. Herein, the relevant researches are summarized, and the properties as well as the performances of ZTCs are compared with those of other materials including metal-organic frameworks, to elucidate the intrinsic advantages of ZTCs and their future development.

1. Introduction

Crystalline microporous materials such as zeolites and metal-organic frameworks (MOFs) possess clearly defined structures at a molecular level, which are advantageous to exhibit size-recognition of molecules, sieving effect, and selective chemical reactions. In addition, the ordered array of nanopores can facilitate mass transfer. Moreover, they can be easily and flexibly functionalized by means of chemical modifications for a variety of applications. In contrast, microporous carbon materials represented by activated carbons generally consist of disordered and defective graphenes which are stacked and/or aggregate,¹ and their structures are far from crystalline form. Their chemical modifications are possible to some extent, but not as controllable as those in the crystalline microporous materials. Nevertheless, the microporous carbon materials possess unique advantages such as chemical stability both in acid and base, thermal stability, hydrophobicity, and electric/thermal conductivity, which cannot be realized in the aforementioned crystalline microporous materials. Therefore, microporous carbon materials have been practically used in a variety of applications as adsorbents, catalysts, catalyst supports and electrode materials for electrochemical capacitors. In this context, if 'crystalline microporous carbons' are realized, they must be very fascinating from the both advantages of these two types of microporous materials. Zeolite-templated carbons (ZTCs) which are featured in this article satisfy such an idea to a great extent, regarding their ordered microporous frameworks and structure regularity. Their unique structural properties^{2,3} and excellent capability for a variety of applications have attracted many

researchers, and over 200 of research papers on ZTCs have been published up to now since the first trial of synthesis by our group.⁴ We had briefly summarized the synthesis techniques and the basic properties of ZTCs as well as their applications in a book chapter in 2012.⁵ Since then, the ZTC research has been remarkably developed, and the update would be beneficial for the researchers working in the relevant field. Moreover, there has been no review paper focusing only on ZTCs and published in a scientific journal. Thus, the purpose of this featured article is to provide a comprehensive review on ZTCs as a journal article, including update of the most recent works.

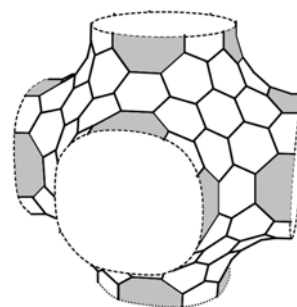


Fig. 1 An example of Mackay crystals. Carbon octagons are coloured. The morphology is categorized to the Schwarz P surface.

Crystalline microporous carbons have been theoretically proposed as Mackay crystals⁶ or carbon Schwarzites⁷ which had emerged as analogy of fullerenes (Fig. 1). Though these imaginary frameworks have never been experimentally synthesized yet, our group has proposed a probable way shown in Fig. 2. In this method, zeolite is used as a template for building a three-dimensional (3D) framework (Fig. 2a).^{4,8-10} Carbon can be introduced into the zeolite nanochannels by means of polymer-impregnation followed by carbonization and/or chemical vapour deposition (CVD) on zeolite

Institute of Multidisciplinary Research for Advanced Materials, Tohoku University, 2-1-1, Katahira, Aoba-ku, Sendai, 980-8577, Japan.
hirotomo.nishihara.b1@tohoku.ac.jp

(Fig. 2b). By removal of zeolite, ZTC is obtained as a negative replica of the parent zeolite (Fig. 2c). Zeolite is an aluminosilicate-based crystalline porous solid. Presently, there are 235 different types of zeolites recorded in the International Zeolite Association, and many of them possess 3D interconnected nanochannels analogical to the inner spaces of the Schwarz minimal surfaces. For example, the channel morphology of FAU zeolite (Fig. 2a; including zeolite Y and X) corresponds to the inner space of the Schwarz D surface, *i.e.*, the diamond-type network structure. While two types of carbon Schwarzites could specifically fit the nanochannels of FAU zeolite (Fig. 3),⁸ the actual ZTC structure has been revealed to have an open-graphene framework as shown in Fig. 4^{8,11} rather than tubular closed-structures like Schwarzites (Figs. 1b, 3c, and 3d). Though ZTC is not a perfect carbon Schwarzite, the framework consists of curved and single-layer nanographenes forming a 3D structure order, making this material distinguishable from other nanoporous carbon materials.

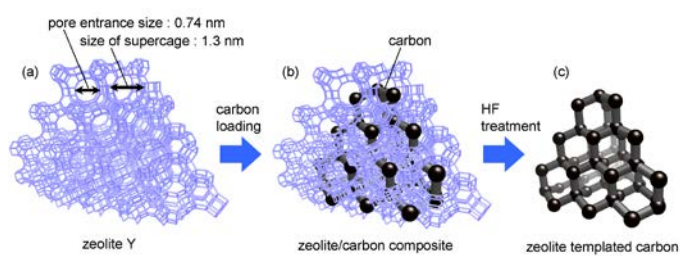


Fig. 2 Synthesis procedure of ZTC. (a) Crystal structure of FAU zeolite (zeolite Y). (b) Illustration of zeolite/carbon composite. A carbon framework formed inside the zeolite channel is shown by a ball-and-stick model. Note that the balls and sticks represent not carbon atoms and C-C bonds, but they represent carbon clusters. (c) Framework structure of the liberated ZTC. Reprinted with permission.⁸ Copyright 2009 Elsevier.

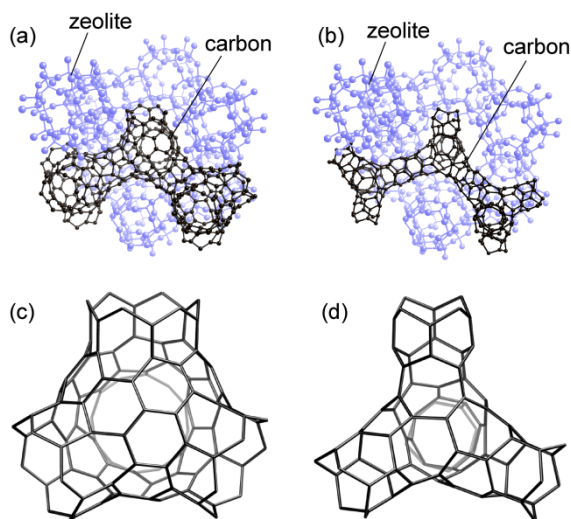


Fig. 3 Two types of carbon Schwarzites which could fit the nanochannels of FAU zeolite. (a) and (b) illustrate the two structures with the zeolite framework, and they consist of (c) C_{68} and (d) C_{68} building units, respectively, both of which include twelve carbon heptagons. Note that one supercage of zeolite Y contains one building unit for both models. Reprinted with permission.⁸ Copyright 2009 Elsevier.

In this featured article, we first describe the development background of ZTCs in the context of the history of the template

carbonization technique, and the structural and chemical diversity of ZTCs are illustrated. Then, a brief summary is given on their capability for applications, including hydrogen storage¹²⁻⁷⁰ and electrochemical capacitors^{25, 71-95}.

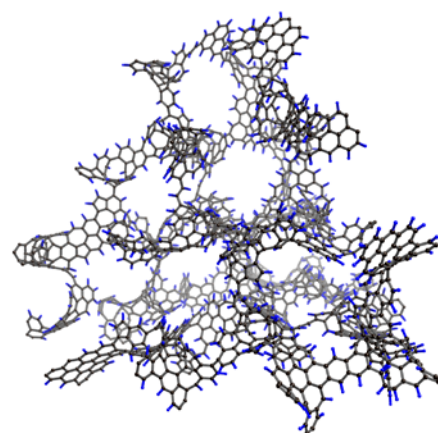


Fig. 4 Structure model of a typical ZTC (Type-I; see 3.1) with a high surface area of ca. $4000 \text{ m}^2 \text{ g}^{-1}$. Reprinted with permission.¹¹ Copyright 2018 Elsevier.

2. Brief history of template carbonization

The major history of the template carbonization is summarized in Fig. 5. The use of template substances for the production of carbon materials began around 1980s. One of the pioneer works was reported by the Knox's group in 1982.⁹⁶ They impregnated silica gels or porous glasses with phenol resin and the resulting mixture was carbonized at 1273 K. After removing the template by alkali, the carbon was heat-treated at 2273-3073 K to obtain porous glassy carbons. In 1987, Pekala *et al.* used porous monoliths prepared by sintering of NaCl particles (ca. $20 \mu\text{m}$) as templates for producing low-density microcellular carbon foams.⁹⁷ In these pioneer works, templates having disordered structures were used.

The first template with a structure regularity was montmorillonite, which is one of the layered clay minerals, reported by our group in 1988.⁹⁸ Though the carbonization of polyacrylonitrile usually yields hard carbons, the carbonization in two-dimensional (2D) nanospace induces the formation of planar graphene sheets, yielding graphite thin films upon the template removal.

In 1995, our group succeeded to extend the templated carbonization to a one-dimensional (1D) template, aluminium anodic oxide (AAO).^{99, 100} AAO is a thin-film porous membrane with cylindrical mesopores which are vertically arrayed to the membrane. The diameter and the length of the mesopores are uniform and controllable. While Martin *et al.* reported the use of AAO template for the production of metal/polymer nanotubes/nanorods in 1994, our group produced multi-walled carbon nanotubes (MWCNTs) with a uniform and controllable diameter and length by CVD. A similar AAO-templated carbonization was reported also by Martin's group in 1998.^{101, 102}

Year	Ref.	Template	Scheme illustration	Obtained carbon	Dimension	Template-derived ordered structure
1982	[96]	Silica gels, Porous glasses		Porous glassy carbons	3D	No
1987	[97]	NaCl		Porous carbons	3D	No
1988	[98]	Montmorillonite		Thin graphite	2D	No
1995	[99]	Anodic Al oxides (AAO)		Carbon nanotubes	1D	No
1998	[101,102]					
1997	[4,103]	Zeolites		ZTCs	3D	Yes
1998	[104]					
2000	[9]					
1998	[105]	Silica opals		Carbon inverse opals	3D	Yes
1999	[106,107]	Mesoporous silicas		Ordered mesoporous carbons	3D	Yes
2004	[108]	Micro-phase separated block copolymers		Ordered mesoporous carbons	3D	Yes
2005	[109,110]	Organic micelle		Ordered mesoporous carbons	3D	Yes
2008	[111]	Metal-organic frameworks		Disordered porous carbons	3D	No
2011	[113]	(MOFs)				
2011	[126]	Ni foam		Macroporous graphene	3D	No
2016	[127]	Al ₂ O ₃ nanoparticles		Mesoporous graphene	3D	No
2017	[125]	Organic crystals		Ordered carbonaceous frameworks	3D	Yes

Fig. 5 Development history of template carbonization and relevant materials.

As mentioned above, 2D (montmorillonite) and 1D (AAO) ordered templates yield 2D and 1D nanocarbons respectively, whereas the resulting nanocarbons are lacking of 3D networks and cannot retain the ordered structures of their parent templates. To obtain 3D ordered carbons, the use of 3D ordered template is necessary. The first attempt of using 3D ordered template was done with zeolite by our group in 1997,⁴ and two methods were proposed: (1) polymer-

impregnation followed by carbonization (an impregnation-carbonization method) and (2) CVD. Soon after our report, the production of ZTCs by the impregnation-carbonization was also reported by Mallouk's group (in 1997)¹⁰³ and the CVD method by Rodriguez-Mirasol's group (in 1998).¹⁰⁴ Unfortunately, these groups did not examine the replication of the zeolite ordered structure at that time. The first ordered porous carbons were reported by

Zakhidov *et al.* in 1998,¹⁰⁵ as carbon inverse opals (CIOs) which were obtained by using silica opals. In 1999, Ryoo's group¹⁰⁶ and Hyeon's group¹⁰⁷ reported the production of ordered mesoporous carbons (OMCs) by using mesoporous silicas as templates. OMCs were the first carbon materials with long-range ordered structures which can be detected by X-ray diffraction (XRD), and had a great impact on the field of porous materials. In 2000, our group finally reported the production of ZTCs with structure regularity derived from zeolite.^{9, 10}

In 2000s, more inexpensive and/or easier soft-template techniques have been developed. Liang *et al.* reported the preparation of OMC films simply by carbonization of block copolymers having a mesoscopic structures formed by microphase separation in 2004.¹⁰⁸ In 2005, Nishiyama's¹⁰⁹ and Meng's¹¹⁰ groups reported the production of OMCs by using surfactant micelles, like the protocol for mesoporous silicas. In these soft-template methods, a nanostructured composite which consists of two phases is first prepared. Specifically, the two phases are (i) a continuous framework phase consisting of thermosetting polymer and (ii) a thermally decomposable phase. By a heat treatment, the former phase turns into a carbon framework, while the latter phase is decomposed and turns into pores. Thus, a 3D ordered carbon is obtained. On the other hand, the development of alternative pathways for ordered microporous carbons has been a challenge.

One of the potential methods is to use organic-based porous crystals such as MOFs as templates or precursors. In 2008, Xu's group reported the use of MOF-5 [Zn₄O(OOCC₆H₄COO)₃] as a template.¹¹¹ Polyfurfuryl alcohol (PFA) was synthesized inside the nanopores of MOF-5, and the composite was carbonized at 1273 K in Ar. Upon the carbonization, ZnO was formed and it turned into Zn (boiling point 1181 K) which can vaporize away. They reported also the use of ZIF-8 as a template.¹¹² However, in both cases, ordered structures of MOFs were completely lost in the final carbon products. A direct conversion of MOFs to porous carbons or composite materials was also attempted^{113, 114} and this has become a trend up to date.¹¹⁵⁻¹²⁴ Nevertheless, none of work had succeeded to retain ordered structures of precursor crystals. In 2017, our group finally succeeded to convert organic crystals into ordered carbonaceous frameworks (OCFs),¹²⁵ in which the precursor crystal is used as a self-template as well as a carbon source. Though the resulting OCFs are poorly porous, OCFs possess ordered frameworks together with molecular-derived functional blocks, exhibiting unique electrocatalysis towards selective CO₂ reduction. The direct conversion technique can extend the controllability of the framework structures in ordered 3D carbonaceous materials.

The template carbonization was applied also for the production of so-called 3D graphene materials. It should be noted that ZTC consists of nano-sized and curved single-layer graphenes having the 3D ordered network, and thus, it can be considered as the first 3D graphene material. In 2011, Cheng's group¹²⁶ produced macroporous graphene networks by using Ni foam as a CVD substrate and a 3D template. The specific surface area of the resulting material is ~850 m² g⁻¹, which is about 1/3 of the theoretical value of single-layer graphene (2627 m² g⁻¹), meaning that ca. 3 layers of graphenes are stacked by average. In 2016, our group reported mesoporous graphene materials by using Al₂O₃

nanoparticles as a template.¹²⁷ Most of framework consists of single-layer graphenes, and the specific surface area achieves 1970 m² g⁻¹. However, these macroporous and mesoporous graphene materials do not have ordered pores. ZTC has been the only graphene-based microporous material with structure regularity.

As is found from Fig. 5, ZTCs were developed at relatively early stage of the history of the template carbonization, and had a great influence on the subsequent researches. However, the amount of relevant papers is not greater than those of OMCs. This is probably because more skilful techniques are required for the synthesis of ZTCs than the cases of OMCs. In the following section, the key factors of synthesis conditions are summarized to reveal proper ways to obtain ZTCs with highly ordered structures.

3. Synthesis of ZTC

3.1 Classification of quality

Even when the same zeolite is used as a template, the resulting ZTC structure could greatly vary depending on the synthesis conditions, especially regarding the degree of ordered structure, and the inclusion of non-templated carbon structures. Thus, it is convenient to define the following three types for ZTCs.

Type-I: ZTCs almost solely consisting of the tree-dimensionally ordered framework replicated by the zeolite template.

Type-II: The mixture of the Type-I structure and extra carbonaceous components, which are non-templated carbon formed outside of zeolite template and/or disordered carbon structures formed by the failure in zeolite replication inside zeolite template.

Type-III: The carbonaceous product which does not (or rarely) contain the Type-I structure. Strictly speaking, Type-III is intrinsically not ZTC, whereas many researchers use the term ZTCs also for such disordered materials. Thus, we refer to this group as Type-III in this article.

Fig. 6 illustrates the three types of ZTCs together with their representative preparation schemes shown as (a)-(l). Examples of TEM images and XRD patterns are given for Type-I, II, and III, and criteria for each type are shown in red-colour font. The explanations of individual schemes are mentioned when necessary at the following text. Type-I is obtained only when the synthesis is carefully performed with appropriate conditions, through the route (e)-(g)-(i) in Fig. 6: uniform carbon introduction only inside the zeolite nanochannels (Fig. 6e), heat treatment at more than 1073 K (Fig. 6g), and template removal (Fig. 6i). The framework thus obtained is nano-sized and curved single-layer graphene forming 3D structure regularity as shown in Fig. 4, without stacking of graphenes. The stacking-free framework exhibits a high geometric surface area at least over 2100 m² g⁻¹.⁸² To be Type-I can be judged by the following experimental data:

- (1) Equipped with an ordered structure derived from zeolite (showing a sharp XRD peak(s) corresponding to zeolite *d*-spacing(s))
- (2) Free from graphene stacking structure (the absence of a carbon 002 XRD peak)
- (3) High surface area (> 2100 m² g⁻¹)

When zeolite ordered-structure is (partially) replicated, Type-II is formed through the route (k)-(l) in Fig. 6: carbon introduction into the zeolite nanochannels along with the formation of the non-templated carbon and/or the failure of zeolite replication (Fig. 6k) and template removal (Fig. 6l). To be Type-II can be judged by the following experimental data:

- (1) Equipped with an ordered structure derived from zeolite
- (2) Presence of graphene stacking structure (showing a carbon 002 XRD peak), or low surface area ($< 2100 \text{ m}^2 \text{ g}^{-1}$)

Type-III is prepared from a variety of pathways (individual pathways are explained in the later chapters), and this is the most frequent (in many cases undesired) product in the ZTC synthesis. To be Type-III can be judged by the following experimental data:

- (1) Absence of an obvious ordered structure derived from zeolite
- In the Type-III ZTCs, an XRD pattern often contains a carbon 002 peak, but this is not mandatory.

The unique properties of ZTCs are derived from the nanographene-based ordered frameworks in Type-I (or partially included in Type-II), and Type-III is intrinsically not very much different from other disordered nanoporous carbons. Therefore, the preparation of Type-I or Type-II is desired for the applications utilizing the unique properties of ZTCs.

3.2 Selection of zeolite framework-type

While 235 types of zeolite frameworks are registered up to now (found in the database provided by the International Zeolite Association), it is important to choose appropriate pore-entrance size as well as the dimension of pore connectivity for obtaining Type-I ZTCs. Table 1 summarises the different types of zeolites used as templates in the ever reported ZTC syntheses. The pore-entrance of zeolite can be simplified by a Si–O–Si ring, and its size is generally classified by the number of oxygen included. Table 1 lists the largest pore entrance size and the dimension of the pore network which are connected through the largest pore-entrance.

It is found that Type-I and -II can be obtained only by using zeolites with a 3D pore network of oxygen 12-membered rings, i.e. BEA,^{16, 18, 46, 53, 70, 72, 76, 81, 87, 103, 128-137} EMT,^{19, 26, 27, 35, 42, 48, 53, 135, 138-145} and FAU.^{2, 4, 8-10, 12-14, 17, 20-23, 25, 27-29, 31, 33, 34, 36-38, 43-69, 71-75, 77, 82, 84, 86-95, 103, 104, 128, 134, 135, 141, 145-218} MFI zeolite has a 3D pore network of oxygen 10-membered rings, but only Type-III has been obtained [(a) in Fig. 6].^{128, 130, 132, 134, 137, 219-225} Thus, it is found that oxygen 10-membered rings are not large enough to build a robust 3D framework without pore-blocking at the carbon introduction step into zeolite.⁵ Also, other zeolites with oxygen 6, 8, and 10-membered rings cannot produce Type-I and Type-II regardless of pore dimension, as is found from the results of AEL,⁷⁹ CHA,^{79, 226, 227} HEU,^{228, 229} IWT,²³⁰ JNT,²³¹ LTA,^{15, 135, 230} MTN,²³² and MWW^{83, 164, 233-235} in Table 1. The dimension of the pore network is another critical factor. As is found in zeolite AFI,²³⁶ LTL,^{103, 130, 135} and MOR,^{130, 134} zeolite ordered-structure can never be replicated by the 1D pore network even

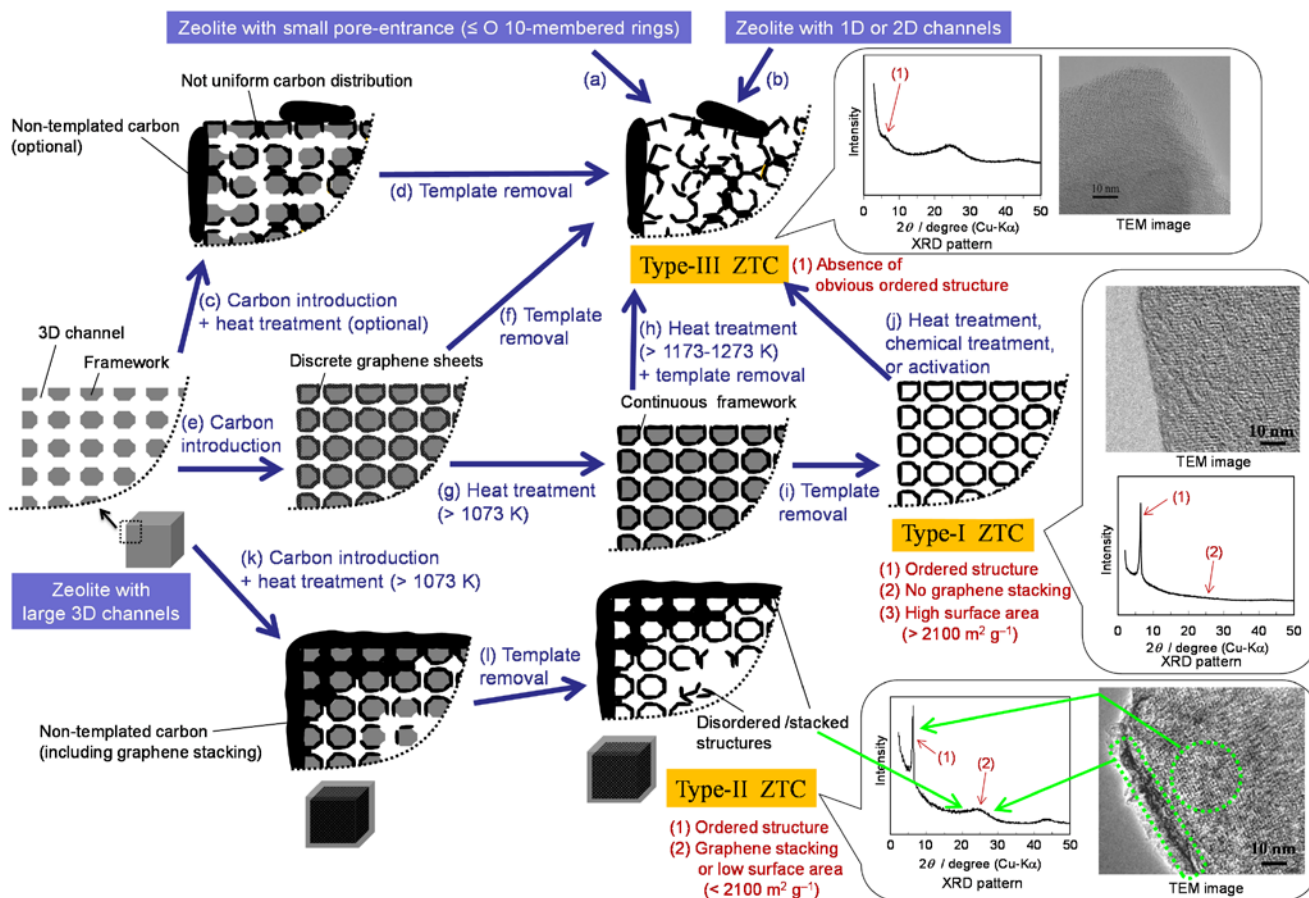


Fig. 6 Classification of ZTC quality into Type-I, II, and III, together with their representative preparation schemes. Each preparation step is labelled with (a) to (l). As examples, XRD patterns and TEM images are shown for representative samples of Type-I, -II, and -III. Criteria for each type are shown in red-colour font.

when the pore-entrance size is large enough [(b) in Fig. 6b]. Also, 2D pore network of oxygen 12-membered rings would yield Type-III, although there has been no report.

As discussed above, a zeolite template must possess a 3D pore network linked through pore entrances over oxygen 12-membered rings to obtain Type-I or Type-II ZTCs. Except the already-reported ones (BEA, EMT, and FAU), promising candidates are BEC, BSV, CLO, IFT, IFU, IRR, IRY, ISV, ITV, IWS, POS, RWY, SAO, SBS, and SBT. If any of the above zeolites can satisfy other necessary requirements (Si/Al ratio and heat-stability) described later, probably new types of ZTCs can be obtained. Among these candidates, only FAU and BEA are commercially available presently. Further, FAU yields ZTCs with a higher degree of structure order, because BEA intrinsically contains disordered moiety. Thus, FAU has been most popularly used for the production of ZTCs so far. EMT can also yield ZTCs with a high degree of structure order, though it is not commercially available. As is found in Table 1, Type-I ZTCs obtained by using FAU and EMT achieve very high Brunauer-Emmett-Teller (BET) surface area (S_{BET}) over 4000 $\text{m}^2 \text{g}^{-1}$.

Most of the commercial synthetic zeolites are not very much cheap, and therefore, inexpensive zeolite templates have been also explored. Natural zeolites generally do not possess large pore-entrance sizes, and, consequently, type-III ZTCs are obtained.^{85, 228, 229, 237} Another approach is to synthesize large-pore zeolite from inexpensive sources such as fly ash and clay.^{60, 61}

Table 1 A list of ZTCs prepared from different types of zeolites.

Zeolite ^a	Pore entrance ^b	Pore dimension ^c	ZTC type	S_{BET}^d ($\text{m}^2 \text{g}^{-1}$)	Ref. ^e
AEL	10	1D	III	975	79
AFI	12	1D	III ^f	—	236
BEA	12	3D	II	2050	130
BEA	12	3D	I	3150	16
CHA	8	3D	III	950	79
EMT	12	3D	I	4120	138
FAU	12	3D	III	2260	4
FAU	12	3D	II	1910	9
FAU	12	3D	I	4100	151
HEU	10	2D	? ^g	405	228
IWT	8	2D	III ^h	—	230
JNT	8	2D	III ^h	—	231
LTA	8	3D	? ^g	410	15
LTL	12	1D	III	121	103
MFI	10	3D	III	690	128
MOR	12	1D	III	180	130
MTN	6	0D	III	269	232
MWW	10	2D	III	1145	233

^a Three-letter code of zeolite which is used as a template. ^b The oxygen number in the Si–O–Si ring corresponding to the largest pore-entrance. ^c Dimension of the pore network which are connected through the largest pore-entrance. ^d BET surface area. ^e References. ^f SWCNTs are formed inside zeolite nanochannels. ^g XRD patterns of ZTCs contain sharp peaks in high-angle region, which seem to be of inorganic impurity. Therefore, it is difficult to judge whether zeolite ordered structure is transferred into ZTC. ^h Carbon nanodots are prepared.

Apart from replicating zeolite ordered-structure, zeolite-template approach can yield also single-walled CNTs (SWCNTs)^{236, 238} and

carbon nanodots showing luminescence property.^{135, 226, 227, 230, 231, 239}

3.3 Si/Al ratio of zeolite

Zeolites have been widely used as solid acid catalysts. The origin of the acid sites is substituted Al in their frameworks. During the long-term use, the acid sites are gradually covered by the deposition of polycyclic aromatic compounds called coke, and catalytic activity becomes degraded. This is so-called poisoning. In the ZTC synthesis, the catalysis for generating coke is positively used for carbon deposition inside the nanochannels of zeolite by CVD. Thus, relatively low Si/Al ratio (high Al content) is required for ZTC synthesis. In our experience, Si/Al less than 20 gives good results.

3.4 Cation type of zeolite

A zeolite Al site has a negative charge, and is balanced by a counter cation. The catalysis of zeolite highly depends on the cation type. For the catalyst applications of zeolite, proton (H) is often used from its high acidity. For ZTC synthesis, however, H-type zeolite is a little difficult to be handled. As described in 3.6, when a common carbon source, furfuryl alcohol (FA), is attached to H-type zeolite, FA is immediately polymerized, and pore blocking occurs, resulting in insufficient impregnation of zeolite with FA. H-type zeolite is often too active also for CVD, and is likely to form non-templated carbon deposition on the outer surface of zeolite particles, yielding Type-II ZTCs.^{14, 82, 146} Nevertheless, Type-II with high surface area ($S_{\text{BET}} = 2750 \text{ m}^2 \text{g}^{-1}$) can be obtained if Si/Al ratio is relatively high (~20) and CVD conditions are properly selected.⁷²

NH_4 -type zeolite has less active than H-type, and it is possible to be homogeneously impregnated with FA. When NH_4 -type zeolite is heated, NH_4 cation is decomposed to release NH_3 and the zeolite turns into H-type. Thus, appropriate CVD conditions should be almost the same as those for H-type zeolite. In addition, NH_4 cation could be a nitrogen (N) source, yielding N-doped ZTCs.^{87, 147} Although Type-I and -II have not been synthesized by using NH_4 -type zeolite,^{21, 22, 37, 44, 46, 50, 59, 65, 87, 134, 147, 153, 163, 171, 186, 190, 240} Type-II ZTCs with high surface area can be prepared in our experience (unpublished data).

Na-type zeolite is commercially available and has been most popularly used from its moderate catalysis which allows homogeneous FA impregnation as well as uniform carbon deposition during CVD. With appropriate conditions, Type-I with a very high $S_{\text{BET}} (> 4000 \text{ m}^2 \text{g}^{-1})$ can be obtained.^{138, 151} An XRD pattern and a TEM image of the Type-I ZTC⁸ are shown in the inset of Fig. 6. There is almost no carbon deposition formed on the outer surface of zeolite particles.^{8, 11} Not only Na, but also other alkali metals and alkaline earth metals can work well. Webley's group reported the production of Type-II ZTCs from zeolite Y with different cations (Na, K, and Ca) by propylene CVD.¹⁴ Zhao's group reported Type-II ZTC with high $S_{\text{BET}} (3331 \text{ m}^2 \text{g}^{-1})$ by using CaX zeolite.⁵⁴ Besides, Ryoo's group reported that CaX zeolite shows larger carbon uptake for CVD with $\text{N}_2/\text{ethylene}/\text{H}_2\text{O}$ flow than NaX zeolite, yielding Type-II ZTC with a high surface area ($S_{\text{BET}} = 2770 \text{ m}^2 \text{g}^{-1}$).²¹⁷ While Na- and K-type zeolites can be easily removed by hydrofluoric acid (HF), Ca-

type yields insoluble CaF_2 . Thus, in the case of Ca-type zeolite, not only HF but also HCl wash is necessary to remove CaF_2 .

Other metal cations have been also investigated. Ryoo's group reported that La-type zeolites (BEA, EMT, and FAU) can yield Type-I ZTCs by ethylene CVD.¹³⁵ Mokaya's group used Pt-type zeolite as a template, and prepared Type-II ZTCs containing well-dispersed Pt nanoparticles.³⁵ On the other hand, zeolites containing transition metal cations such as Ni^{2+} and Co^{2+} function as catalysts for CNT growth^{241, 242} upon CVD, being not appropriate as templates for ZTCs.

3.5 Heat-stability of zeolite

To replicate zeolite ordered-structure, a carbon framework formed inside zeolite nanochannels has to be strengthened by a post high-temperature treatment at least above 1073 K [(g) and (k) in Fig. 6],^{146, 218} and preferably above 1123 K in our experience. Therefore, zeolite template needs to be stable up to 1073–1123 K when its nanochannels contain carbon. Note that zeolite thermal stability is slightly improved up to ca. 1173–1273 K, by the incorporation of carbon. Above the upper limit temperature of zeolite, only Type-III ZTCs are obtained [(h) in Fig. 6] as mentioned in 3.7.

3.6 Carbon introduction methods into zeolites

There are the following three major methods for the carbon introduction into zeolite nanochannels:

(1) Impregnation-carbonization method

In this method, an organic monomer(s) is introduced into zeolite channels, and it is polymerized to form polymer/zeolite composite. Since zeolite catalysis can convert most of organic compound into polymers and then carbonaceous substance, it is possible to use a variety of monomers including the ones which are not used for general polymer synthesis. In addition, polymerization without zeolite catalysis is also possible, for example by the irradiation of γ -ray to acrylonitrile monomers in zeolite channels.⁴ The monomer introduction can be achieved via vapour^{148, 156, 212, 213} or liquid phases. As for the latter, a variety of monomers has been examined thus far: FA,⁴ acrylonitrile,⁴ phenol-formaldehyde,¹⁰³ vinyl acetate,¹²⁸ pyrene,¹²⁸ sucrose,¹⁵³ poly(styrene sulfonic acid-co-maleic acid) sodium salt,²¹⁰ poly(styrene-co-maleic acid) partial isobutyl/methyl mixed ester,²¹⁰ ethylene diamine,^{75, 164} 2-thiophenemethanol,¹⁴³ lignin,^{87, 134} pitch,⁸⁷ glucose,¹⁹⁸ and an ionic liquid, 1-ethyl-3-methylimidazolium tetracyanoborate (EMIT).⁹⁴ Among the monomers reported so far, FA has been the most popular. Liquid FA is easily introduced into zeolite channels with a vacuum impregnation technique. Extra FA remaining the outside of zeolite can be removed by solvent with a larger molecular size than the pore-entrance size of zeolite, for example mesitylene for FAU zeolite.⁴ A mild annealing at 423 K can polymerize FA into polyfurfuryl alcohol (PFA) inside zeolite nanochannels by the zeolite acid catalysis. However, the carbon yield of polymers upon carbonization inside zeolite is relatively low (ca. 30 wt%), and the resulting carbon loading amount is not large enough (usually < 15 wt%) to build a robust framework which can retain the zeolite ordered structure upon the template removal. Thus, this

impregnation-carbonization method usually generates Type-III ZTCs through the route (c)-(d) in Fig. 6: insufficient carbon introduction (Fig. 6c) and template removal (Fig. 6d).

(2) CVD

CVD^{4, 103} is an essential process to introduce an enough large amount of carbon into zeolite to obtain Type-I and -II ZTCs. Since the zeolite pore-entrance size is narrowed by the carbon deposition, CVD source molecules should be very small. For example, styrene¹³² and benzene¹⁷⁵ are too large. The synthesis of Type-II ZTCs has been reported by using methane,¹⁹³ ethylene,²⁷ propylene,¹³⁰ butylene,¹⁴ and acetonitrile (AN).^{16, 132} Type-I ZTCs can be obtained with acetylene CVD simply by a single step on commercial zeolite.¹⁵⁰ Moreover, a two-step CVD at different temperatures can yield Type-I ZTCs with high surface areas (up to $3370 \text{ m}^2 \text{ g}^{-1}$).¹⁵⁰ Ryoo's group reported that Type-I and -II ZTCs can be easily synthesized by introducing a small amount of water-vapour during a CVD process using AN¹³⁶ or ethylene²¹⁷ as a source gas. Also, they have discovered that ion-exchange of zeolite with La^{135} or Ca^{217} is effective to easily produce Type-I and -II ZTCs by ethylene-CVD.

As described in 3.3, zeolite catalysis for coke deposition is necessary for homogeneous carbon deposition. With the zeolite catalysis, CVD source gas is decomposed and turned into carbon inside zeolite nanochannels. A key point of the CVD process is the selection of temperature. Each CVD source gas has its thermal decomposition temperature above which the gas turns into carbon (soot) in gas phase even without any catalyst. For example, the decomposition temperatures of acetylene and propylene are ca. 923 K and 1023 K, respectively. Above the decomposition temperature, carbon is deposited not only inside but also the outside of zeolite particles, giving rise to the formation of Type-II ZTC containing non-templated carbon deposition. Accordingly, CVD temperature should be lower than the decomposition temperature to obtain Type-I ZTCs. By such CVD conditions, polycyclic aromatic compounds are generated inside zeolite nanochannels, whereas they are not robustly connected each other yet.²¹⁸ Therefore, upon the template removal, Type-III ZTCs are formed (the route (e)-(f) in Fig. 6). Above 1073–1123 K, the polycyclic aromatic compounds are condensed to form a continuous carbon framework which can retain the ordered structure of zeolite even upon the zeolite removal.²¹⁸ Thus, a CVD process needs to be followed by a high-temperature heat treatment (<1073–1123 K) when the CVD temperature is below 1073 K. The one-step carbon introduction by CVD can produce Type-I ZTCs although S_{BET} is not as high as those obtained by the following two-step method. For mass production, CVD is advantageous.^{135, 214, 217}

(3) Two-step method

This method is the combination of (1) and (2). In most of the cases, FA is used for (1), and the subsequent CVD is performed with acetylene,¹⁶⁶ ethylene,²⁷ propylene,⁹ butylene,¹⁷³ benzene,¹⁵⁴ or AN¹⁴⁹ as a source gas. Also, some combinations have been reported: (1) lignin and (2) acetylene,¹³⁴ and (1) methanol and (2) 2-methylfuran.¹³⁷ Type-I ZTCs with S_{BET} over $4000 \text{ m}^2 \text{ g}^{-1}$ have been synthesized only by using the two-step method,^{138, 151} probably because of very uniform carbon introduction throughout the zeolite particles.

3.7 Porosity development methods

One of the advantages of ZTCs is their large surface areas as well as uniform and ordered micropores. However, the porosity actually varies depending on the preparation method and additional activation. Herein, several methods for porosity development are summarized.

(1) Zeolite replication

This is the most straightforward method to develop micropores in the ZTC synthesis, and a proper replication yields Type-I ZTCs. Fig. 4 shows the framework structure of this type of ZTCs.¹¹ The porosity accords with the space which was originally occupied by zeolite framework, and therefore, an ordered microporous network with uniform size (typically ca. 1.2 nm) can be obtained, and the entire porosity should consist solely of micropores (micropore volume is ca. 1.8–1.9 cm³ g⁻¹)^{11, 138, 151} The highest S_{BET} achieved in this type of ZTCs is ~4000 m² g⁻¹.^{138, 151}

The ordered microporosity can be formed also in the case of Type-II, though it may contain non-uniform pores. Additionally, a non-templated carbon deposition is almost non-porous and lowers its porosity. When zeolite replication is (mostly) failed, Type-III ZTCs are formed. The porosity of such ZTC is significantly disordered, and not distinguishable from ordinary porous carbons like activated carbons.

(2) Thermal collapse of zeolite

When a carbon/zeolite composite is heat-treated above the stability limit temperature of zeolite (1173–1273 K), zeolite is transformed into a disordered framework which still functions as a template for generating disordered nanopores. Thus, Type-III ZTC can be obtained by removing the template (Fig. 6h).^{21, 22, 63, 147, 153, 163, 186} This method easily provides highly porous carbons: S_{BET} can be as high as 3683 m² g⁻¹.¹⁴⁷

(3) Activation of ZTCs

When the original ZTCs are Type-II and -III which are not highly porous, activation can improve the porosity. Thus, the activation of ZTCs has been reported with CO₂,⁷⁵ KOH,^{25, 31, 44, 75, 137} and H₃PO₄.⁴⁴ Nevertheless, the highest S_{BET} reported so far is 3064 m² g⁻¹,³¹ still not as high as the maximum in Type-I ZTCs (~4000 m² g⁻¹). Activation process involves oxidative gasification of a carbon framework to form CO and CO₂, resulting in the destruction of carbonaceous framework depending on the degree of activation. Thus, the activated ZTCs are likely to be Type-III [(j) in Fig. 6]. Note that activation of Type-I ZTC is not effective, because it has already fully porous framework (Fig. 4), and oxidative gasification of the framework results in the decrease of surface area owing to restacking of graphenes. Moreover, the Type-I ZTC framework is not very much stable at a temperature used for activation (> 873 K). Type-I ZTC is stable up to ca. 673 K,⁹¹ and its porosity is gradually decreased along with the temperature above 673 K.

Among the methods (1) to (3) described above, (1) for highly porous Type-I/-II ZTCs can yield the materials which are equipped with a unique nanographene-based framework like the one shown in Fig. 4. Moreover, Type-I/-II ZTCs which are properly synthesized can achieve high porosity with surface area over 3000 m² g⁻¹. On the other hand, the advantages of methods (2) and (3) are ease of

preparation and the introduction of significant mesoporosity. However, the resulting carbons are not greatly different from highly activated carbons which have very high S_{BET} (>3000 m² g⁻¹) as well as a significant mesoporosity.

4. Structure of ZTC and its extension

4.1 Atomistic structure of Type-I ZTC

Although the first ZTC was reported as early as in 1997,^{4, 103} the atomistic structure of Type-I ZTC has been unknown over years. In 2006, Roussel *et al.* proposed framework models which have tube-like closed graphene frameworks and resemble Mackay crystals or carbon Schwarzites.^{158, 161} However, their models consist of too many carbon atoms. When their models are embedded in FAU zeolite, the carbon content (w_c) becomes 0.62–0.73 g-carbon g⁻¹-zeolite, and these values are far larger than the case of a typical Type-I ZTC (0.29 g g⁻¹). Ryoo's group also proposed a similar framework model for Type-I ZTC, but such a tubular framework needs too many carbon atoms and is inconsistent with the measured w_c value (0.30 g g⁻¹) of their Type-I ZTC.¹³⁵ We proposed that a structure consisting of an open-graphene framework rather than closed tubular ones can realize a stable 3D network with realistic number of carbon atoms ($w_c = 0.29$ g g⁻¹) in 2009.⁸ Most recently, we have updated the structure model with the one shown in Fig. 4, as a more realistic model including structure disorder and irregular.¹¹ Curved and non-stacked graphene fragments are connected along the ordered zeolite nanochannels, forming a long-range structure order. The framework contains a diverse range of carbon polygons such as hexagons, heptagons and octagons, while pentagons are minor. The presence of carbon heptagons and octagons resembles Mackay crystals and carbon Schwarzites.

4.2 ZTC as a 3D graphene material

The 3D framework consisting of single-layer graphene without stacking is valuable to achieve a high surface area. Fig. 7 summarizes geometric (theoretical) and measured surface areas of representative nanocarbons: C₆₀, SWCNT, graphene, and ZTC. Their morphologies are 0D, 1D, 2D, and 3D, respectively. The outside surface area of a single C₆₀ molecule is as high as 2625 m² g⁻¹, whereas C₆₀ actually forms an fcc crystal and its surface area is almost 0 m² g⁻¹, because most of the molecular surface is hidden inside the crystal. SWCNT also has a high outside surface area depending on its diameter. For example, SWCNTs with 1 nm and 3 nm in diameter have geometric surface areas of 1760 and 1460 m² g⁻¹, respectively. However, the measured values are at most ca. 1000 m² g⁻¹,²⁴³ because of bundling. Graphene is also well known to have a high geometric surface area of 2627 m² g⁻¹, whereas the measured value is ca. 700 m² g⁻¹ because of stacking.²⁴⁴ Thus, 0D, 1D, and 2D structures inevitably cause unfavourable surface loss. To fully expose the entire surface of graphene, a self-standing open 3D framework is necessary, and ZTC does realize this ideal. The high geometric surface area of ZTC (3707 m² g⁻¹) exceeding the value of graphene (2627 m² g⁻¹) is because of the significant contribution of the edge planes.⁵ Fig. 8 illustrates the geometric surface areas of graphene (Fig. 8a), polycyclic aromatic compounds (Figs. 8b and c), and one benzene molecule (Fig. 8d). For infinitely large graphene, the contribution of edge planes can be ignored, whereas it becomes

significant at nano-sized graphenes. As shown in Figs. 8b-d, the specific surface area is increased with decreasing graphene-domain size because of the increasing contribution of the edge plane. Indeed, the width of the ZTC graphene framework is ca. 1 nm, similar to coronene (Fig. 8c), although the ZTC framework is continuous (like ribbon) and the geometrical surface area is lower than that of coronene. Unlike other low dimensional nanocarbons, ZTC with a 3D graphene framework is free from graphene aggregation/stacking, and the experimentally measured surface area ($3730 \text{ m}^2 \text{ g}^{-1}$ by the subtracting pore effect method²⁴⁵) is almost the same as the geometric one.

Recently, so-called "3D graphene" or "porous graphene" materials have been intensively investigated.^{126, 246-253} However, most of them have much lower surface area ($< 1000 \text{ m}^2 \text{ g}^{-1}$) than the geometric value ($2627 \text{ m}^2 \text{ g}^{-1}$) because of the graphene stacking.

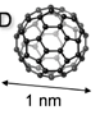
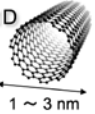
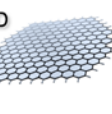
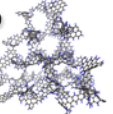
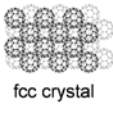
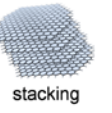
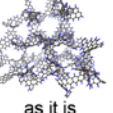
	C_{60}	SWCNT	Graphene	ZTC
Unit	0D 	1D 	2D 	3D 
Geometrical surface area	$2625 \text{ m}^2/\text{g}$ (outside only)	$1460 \sim 1760 \text{ m}^2/\text{g}$ (outside only)	$2627 \text{ m}^2/\text{g}$ (both sides)	$3707 \text{ m}^2/\text{g}$ ¹¹ (both sides+edge)
Actual structure	fcc crystal 	bundle 	stacking 	as it is 
Measured surface area	$\sim 0 \text{ m}^2/\text{g}$	$\sim 1000 \text{ m}^2/\text{g}$ ²⁴³	$\sim 700 \text{ m}^2/\text{g}$ ²⁴⁴	$\sim 3730 \text{ m}^2/\text{g}$ ⁸

Fig. 7 Unit structures (upper) and actual structures (bottom) together with geometric surface areas and measured surface areas, respectively, for C_{60} , SWCNT, graphene, and ZTC.

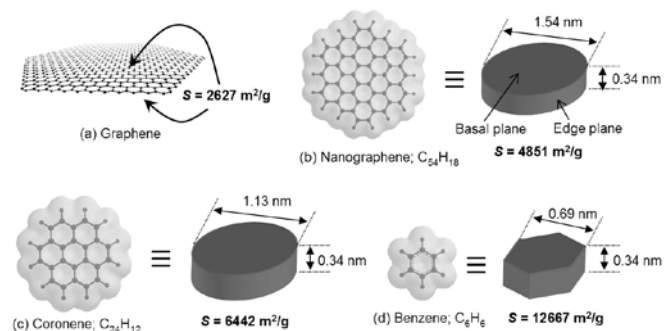


Fig. 8 Molecular models and the corresponding geometric surface areas (S) of (a) graphene, (b) nanographene ($\text{C}_{54}\text{H}_{18}$), (c) coronene, and (d) benzene. Reprinted with permission.⁵ Copyright 2012 Elsevier.

The 3D graphene framework inherits the mechanical elasticity and strength of graphene,²⁵⁴ even in the form of a nanoporous material. The bulk modulus of Type-I ZTC is 0.51 GPa, much lower than zeolite (13 GPa) and MOF ZIF-8 (9.2 GPa).¹⁸³ Thus, ZTC is mechanically very soft, and it is possible to precisely control the average micropore size by hot pressing (Fig. 9).¹⁵⁹ Moreover, ZTC can be reversibly compressed/recovered by mechanical force like a plastic sponge. By using such elastic nanoporous materials, we have proposed an advanced adsorption control as shown in Fig. 10.¹⁸³ By loading mechanical force to a nanoporous material, the nanopores

are contracted, and the physisorption potential is increased, which is expected to enhance molecular adsorption (from Fig. 9a to b). Further contraction results in reducing the adsorption amount (from Fig. 10b to c). When the applied force is gradually released, the nanopores and the corresponding adsorption amount are recovered up to the original state (from Fig. 10c, b, and to a). We have indeed demonstrated a part of this idea by using ZTC¹⁸³ and also by using graphene mesosponge,¹²⁷ which is another 3D graphene material with significant elasticity.

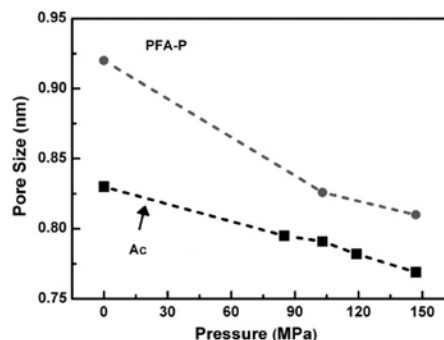


Fig. 9 Plots of average micropore size against pressure in the hot-pressing at 573 K. PFA-P: Type-I ZTC, Ac: a reference activated carbon. Reprinted with permission.¹⁵⁹ Copyright 2007 Elsevier.

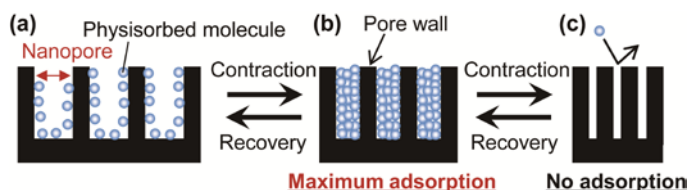


Fig. 10 Illustration for the continuous and reversible pore-size control by loading mechanical force, and the resulting change in molecular physisorption amount. Reprinted with permission.¹⁸³ Copyright 2013 Wiley.

4.3 Structure variation of Type-I ZTC

In the Type-I ZTC with very high S_{BET} ($\sim 4000 \text{ m}^2 \text{ g}^{-1}$), w_c (the amount of carbon introduced in 1 g of zeolite) is 0.29 g g^{-1} .⁸ This is almost the minimal carbon introduction amount which can retain a self-standing ordered framework. In other words, such ZTC comprises of the thinnest nanographene framework. When w_c is increased, the framework becomes thicker and surface area decreases. Instead, electric conductivity is increased.⁷⁷

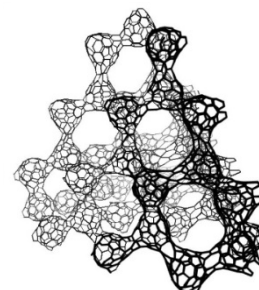


Fig. 11 Structure model of ZTC with $w_c = 0.54 \text{ g g}^{-1}$. Reprinted with permission.⁸² Copyright 2013 Elsevier.

We have tried to introduce carbon into FAU zeolite as much as possible by means of a pressure-pulsed CVD, and found that 0.54 g

g^{-1} is almost the achievable upper limit which can be introduced inside zeolite nanochannels.⁸² In this case, Type-II ZTC is obtained, and it consists of a crosslinked fullerene-like framework (Fig. 11) formed inside zeolite nanochannels, and a thick outside carbon shell. S_{BET} of only the fullerene-like framework was measured to be $1950 \text{ m}^2 \text{ g}^{-1}$, close to the corresponding geometrical value ($2100 \text{ m}^2 \text{ g}^{-1}$).

4.4 Chemical modification

Type-I ZTC possesses about 10-times larger amount of edge sites than conventional activated carbons.⁸⁴ Moreover, the edge sites of ZTC is more reactive than those of other carbon materials.⁸⁴ Thus, chemical modification of ZTCs has been investigated so far by means of oxygen-plasma treatment,³³ modified hydroboration,⁹¹ sulfonation,¹⁸² fluorination,¹⁹⁵ and bromination.²⁰⁰

Chemical modification is possible not only directly on ZTCs, but also on their precursors, i.e. carbon/zeolite composites. We have revealed that many of carbon edge sites are not terminated by hydrogen and exist as dangling bonds at the stage of the carbon/zeolite composite.²¹⁸ Thus, it is possible to modify such dangling bonds for example by a high-temperature gas treatment with H_2 ²¹⁸ and H_2S .⁷⁰ Note that the dangling bonds are naturally terminated by oxygen-functional groups when they are exposed to O_2 and/or H_2O upon template removal. Thus, ZTCs usually contain a relatively large amount of oxygen (O), about 6-9 wt%.^{8, 218}

While the chemical modification is often too harsh for the ZTC framework, electrochemical modification proceeds in milder conditions, enabling the retention of the ordered framework. Berenguer *et al.* reported that the edge sites of ZTCs are effectively oxidized by electrochemical oxidation in an aqueous electrolyte (Fig. 12).¹⁸¹ Moreover, our group have revealed that the electrochemical oxidation in H_2SO_4 can introduce a large amount of quinone-type groups showing a large pseudocapacitance ($\sim 500 \text{ F g}^{-1}$; see 5.5.2) with a high selectivity of ca. 36%, compared to the case of conventional chemical oxidation on activated carbon (ca. 5.2%).⁸⁴ González *et al.* demonstrated the electrochemical functionalization of ZTC with aminobenzene acids in an aqueous electrolyte.⁹⁰ Further, our group have reported that ZTC edge sites can be oxidized also in an organic electrolyte, and redox active quinone and furan-type ether groups can be introduced to exhibit a large pseudocapacitance up to $\sim 330 \text{ F g}^{-1}$ (see 5.5.3).

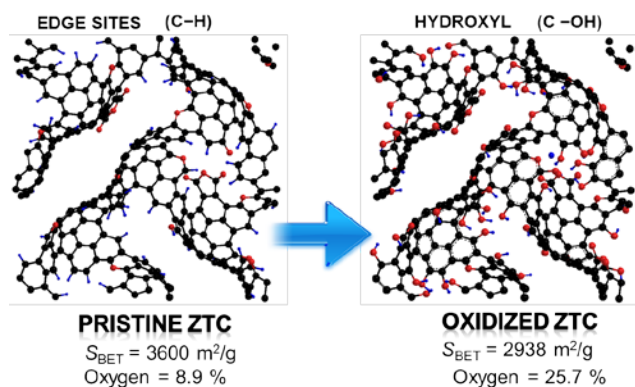


Fig. 12 Schematic for electrochemical oxidation of ZTC. Reprinted with permission.¹⁸¹ Copyright 2013 Elsevier.

4.5 Heteroatom doping

The function of ZTC can be extended also by heteroatom-doping. Not only O-doping mentioned above, but also doping by other heteroatoms such as nitrogen (N), boron (B), and sulfur (S) has been reported.

4.5.1 N-doping

There have been many reports on N-doping into ZTCs.^{12, 16, 18, 23, 50, 71, 73, 87, 91, 132, 136, 140, 145, 147, 149, 156, 161, 180, 219, 232, 234} The N-doped ZTCs prepared by different methods are listed in Table 2. Su *et al.* synthesized N-doped ZTCs simply by using NH_4 -type zeolite as a template and a N source in 2004.¹⁴⁷ They applied the impregnation-carbonization method with FA as a carbon source, and Type-III ZTCs were obtained. Regarding to the impregnation-carbonization method, our group used acrylonitrile in 1997,¹⁰³ Garsuch *et al.* used pyrrole,¹⁵⁶ and Ruiz *et al.* used lignin.⁸⁷

Mokaya's group used AN as a N-containing CVD source on BEA zeolite, and obtained Type-II ZTCs doped with N in 2005.^{16, 132} The similar AN-CVD has been applied to FAU and MET zeolites by Portet *et al.*⁷³ and Wang *et al.*,¹⁴⁵ respectively. Ryoo's groups has reported that the mixture gas of AN and H_2O vapor can also yield Type-II ZTC.¹³⁶

Hou *et al.* developed the two-step method using FA and AN as a primal carbon source and a N-containing CVD source, respectively, to obtain the first Type-I ZTCs doped with N in 2005.¹⁴⁹ Ania *et al.* also reported a two-step method consisting of polymerization of acrylonitrile (ACN) in zeolite, followed by propylene CVD, and obtained Type-II ZTC doped with N.⁷¹ As is found from Table 2, N content is ca. 3-7, and S_{BET} varies in the range of ca. $900\text{-}3700 \text{ m}^2 \text{ g}^{-1}$.

N-doping is effective to improve hydrophilicity,¹⁴⁹ electric conductivity,⁹¹ electrochemical capacitance,^{71, 87} and electrocatalysis for oxygen-reduction reaction (ORR),^{94, 136} while it is not effective to enhance H_2 physisorption at room temperature.²³

Table 2 A list of N-doped ZTCs prepared by different methods.

Zeolite ^a	N-source	ZTC type	N% ^b	N/C ^b	S_{BET} ($\text{m}^2 \text{ g}^{-1}$)	Ref.
NH_4 -FAU	NH_4^+	III	1.84	0.019	3683	147
NH_4 -FAU	NH_4^+	III	5.90	0.064	1749	147
H-FAU	pyrrole	–	5-7	0.054-0.076	900	156
NH_4 -FAU	NH_4^+ , lignin	III	2.8	0.030	950	87
BEA	AN	II	3.2	–	2272	132
FAU	AN	II	7.2	0.068	1987	73
Na-EMT	AN	–	6-7	–	2559	145
H-BEA	AN	II	3.8	–	1860	136
Na-FAU	AN	I	6	0.058	3310	149
Na-FAU	ACN	II	6.0	0.062	1680	71

^a Type of zeolite used as template. A prefix expressing the cation type is described if it is found in the literature. ^b N mass ratio (wt%) and N/C atomic ratio (appeared as N% and N/C, respectively) determined by bulk elemental analysis.

4.5.2 BN-doping

The introduction of B into porous carbons is generally difficult, because B has an unoccupied orbital and is very likely to react with O, which usually exists in chemical/physical activation processes. Thus, there have been only three reports on ZTCs shown in Table 3, and all of them are accompanied with N-doping.

Wang *et al.* reported the introduction of B and N into ZTC via a post-treatment of Type-I ZTC with B_2O_3 and NH_3 at 1423 K. By the harsh treatment, the ordered structure was totally destroyed, and the resulting BN-doped ZTC was Type-III. Nevertheless, the BN-doped ZTC exhibited enhanced hydrogen storage through a spillover mechanism induced by Ru nanoparticles (see 5.2). Our group fabricated Type-I BN-doped ZTC by a modified hydroboration using dimethylamine borane (DMAB) as a BN-source.⁹¹ Most of B was doped in the form of $-B(OH)_2$, and we found that $-B(OH)_2$ group has no enhancement effect on the electrochemical property of ZTC. Further, our group synthesized Type-II BN-doped ZTCs with high surface areas using an ionic liquid, EMIT, as a BN source (Fig. 13). Compared with N-doped ZTC, BN-doped ZTC exhibited better catalysis for ORR, whereas BN-doping was found to be less effective to increase the electrochemical capacitance than N-doping.

Table 3 A list of BN-doped ZTCs.

Zeolite ^a	B-source	ZTC type	B/C ^b	N/C ^b	S_{BET} ($m^2 g^{-1}$)	Ref.
Na-FAU	B_2O_3	III	0.141	0.156	953	26
Na-FAU	DMAB	I	0.010	0.002	3280	91
Na-FAU	EMIT	II	0.026	0.045	1846	94

^a Type of zeolite used as template. A prefix expresses the cation type. ^b B/C or N/C atomic ratio measured by X-ray photoelectron spectroscopy (XPS).

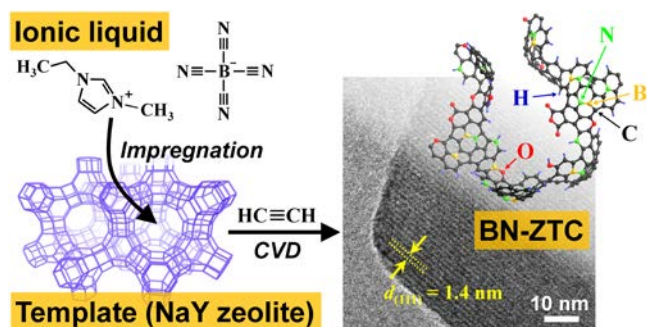


Fig. 13 Schematic for the synthesis of BN-doped ZTC by using EMIT as a BN source. Reprinted with permission.⁹⁴ Copyright 2017 The Royal Society of Chemistry.

4.5.3 S-doping

S-doping has been also reported by several different ways as listed in Table 4. Xia *et al.* synthesized Type-II ZTCs doped with S by a two-step method in which EMT zeolite impregnated with 2-thiophenemethanol (2TM) was heat-treated, followed by ethylene-CVD.¹⁴³ They have reported that S-doped ZTCs exhibited enhanced heat of adsorption for H_2 and CO_2 . Fukuhara *et al.* introduced $-SO_3H$ groups into ZTCs by a post-treatment with chlorosulfuric acid (CSA).¹⁸² The resulting sulfonated ZTCs (Type-III) exhibited enhanced catalysis for hydrolysis of cellobiose and the Beckmann rearrangement. Choi *et al.* synthesized highly S-doped (17 wt%) ZTC

by using a gas mixture of acetylene/ H_2S for CVD at 823 K on NaX zeolite, followed by a heat-treatment in a gas mixture of He/H_2S at 1073 K.²¹⁵ A large amount of S sites can accommodate Pt to achieve its high dispersion (Fig. 14), and the Pt-loaded S-doped ZTC exhibited a unique electrocatalysis for ORR. A similar method has been reported also by Martínez de Yuso *et al.*⁷⁰ A propylene-CVD was performed at 973 K on zeolite H β , and then the gas was switched to pure H_2S for S-doping. They reported that S-doping was effective for hydrogen and CO_2 storage, as was reported also by Xia *et al.*

Table 4 A list of S-doped ZTCs.

Zeolite ^a	S-source	ZTC type	S content ^b (wt%)	S_{BET} ($m^2 g^{-1}$)	Ref.
Na-EMT	2TM	II	2.0 (XPS)	1627	143
FAU	CSA	III	3.4 (EA)	890	182
Na-FAU	H_2S	– ^c	17 (EA)	2770	215
H-BEA	H_2S	II	10.2 (XPS)	2542	70

^a Type of zeolite used as template. A prefix expressing the cation type is described if it is found in the literature. ^b S mass content determined by the method shown in parenthesis: EA (elemental analysis) or XPS. ^c No data are found about ordered structure.

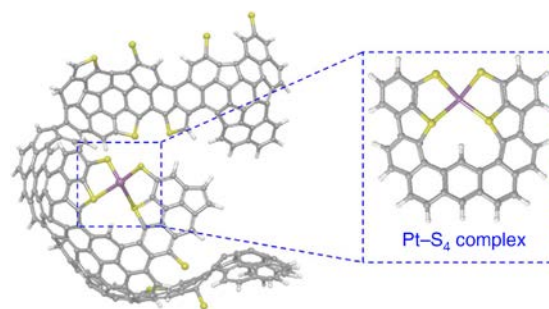


Fig. 14 A structure model of S-doped ZTC accommodating Pt. Reprinted with permission.²¹⁵ Copyright 2016 Nature Publishing Group.

4.6 Composites

The introduction of other substances into the nanochannels of ZTCs has been investigated to extend the versatility of ZTCs as follows.

Metal: Pt,^{17, 19, 20, 23, 28, 33, 35, 43, 48, 57, 69, 154, 174, 177, 178, 188, 191, 208, 209, 215}
 Pt-Ru,¹⁹² Cu,²¹¹ Co,²¹¹ Fe,²¹¹ Ru,^{19, 26} Ni,¹⁹ Pd,^{20, 38, 51} Ir,^{20, 178} Rh,^{20, 178}
 and Ag.^{20, 178}

Metal oxide: TiO_2 ¹⁸⁹ and Fe_3O_4 .^{222, 223, 225}

Others: $LiBH_4$,⁶² sulfur,²¹⁶ and quinone molecules.²⁰³

ZTCs decorated with metal nanoparticles have been applied to methanol oxidation,^{154, 174, 192} ORR,^{177, 188, 208, 209} separation,²¹¹ hydrogen storage,^{17, 19} and catalytic hydrogenation,¹⁹¹ and exhibited superior performances to conventional materials from their highly developed porosity and good mass transport property. While it is easy to disperse small metal nanoparticles (3-6 nm) in ZTC by using conventional metal-loading methods,^{19, 154} anchor site introduction (Fig. 14)²¹⁵ or the use of an organometallic complex as a metal source (Fig. 15)⁶⁹ can achieve subnanocluster dispersion and even single-atom dispersion. A TiO_2/ZTC composite showed superior photocatalysis due to the excellent adsorption capacity of ZTC, and

$\text{Fe}_3\text{O}_4/\text{ZTC}$ composites could be used as adsorbents which can be easily collected by magnet.^{222, 223, 225} LiBH_4 confined in ZTC nanopores showed better cyclability for hydrogen storage than bulk LiBH_4 .⁶² Sulfur-loaded (46 wt%) ZTC functioned as a cathode for Li-S batteries.²¹⁶ Nueangnoraj *et al.* assembled a stable organic proton battery by using ZTCs loaded with two different types of quinones as a positive and a negative electrode.²⁰³

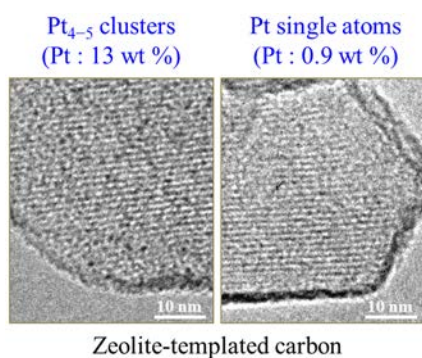


Fig. 15 TEM images of ZTCs loaded with Pt_{4-5} clusters and Pt single atoms. Reprinted with permission.⁶⁹ Copyright 2017 American Chemical Society.

When preparing ZTC-based composites, it is necessary to be careful about the stability of ZTC at the compositing process. Type-I ZTC is thermally stable up to 673 K under inert atmosphere despite the desorption of thermally weak oxygen-functional groups,⁹¹ whereas the ZTC framework gradually collapses above 673 K. In our experience, ZTC is not very much stable in basic media and also in oxidizing conditions. The compositing conditions need to be selected to avoid the structure collapse of ZTC as much as possible.

4.7 Exterior shape

The control of exterior shape is important for most of applications. In principle, the particle shape of ZTC accords with that of its template. As shown in Fig. 16, the bulk shapes of the zeolite templates are well transferred to those of the corresponding ZTCs.¹⁵⁵ Moreover, if zeolite template is molded into a certain shape, it is transferred into the resulting ZTC. According to this mechanism, a variety of exterior shapes have been reported: spherical beads,¹³¹ pellet,^{64, 160} thin film,⁸⁰ core-shell particles composed of ZTC core and mesoporous shell,^{185, 190} monolithic foam,²²⁰ and various forms of monoliths.²⁰¹

Pelletization is possible also by direct pressing of ZTC powder with¹⁶³ and without^{159, 171} binders (Fig. 17). For many of applications, not only gravimetric surface area, e.g. S_{BET} [$\text{m}^2 \text{g}^{-1}$], but also volumetric surface area, S_v [$\text{m}^2 \text{cm}^{-3}$], is of great importance.

S_v can be calculated by the following equation:

$$S_v = S_g \rho \quad (1)$$

where S_g [$\text{m}^2 \text{g}^{-1}$] and ρ [g cm^{-3}] are gravimetric surface area and density of pellet, respectively. There are several different methods to obtain S_g , and BET surface area (S_{BET}) is most popularly used as S_g . For obtaining S_v of powdery sample, tap density is used for ρ . Indeed, reported S_v values of pelletized ZTCs in literature are found to be calculated from S_{BET} and ρ (Table 5). However, the density of pellet (ρ) is often significantly overestimated, causing overestimation of S_v . This can be revealed by calculating the

theoretical maximum volumetric surface area ($S_{v-\text{max}}$) based on S_{BET} and the theoretical maximum density (ρ_{max}) as follows.

$$S_{v-\text{max}} = S_{\text{BET}} \rho_{\text{max}} \quad (2)$$

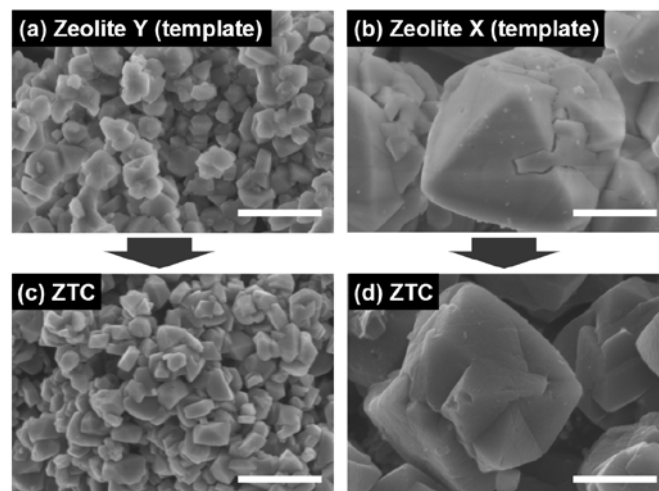


Fig. 16 SEM images of (a) zeolite Y (particle size is ca. 200 nm), (b) zeolite X (particle size is ca. 2 μm), (c) ZTC from zeolite Y and (d) ZTC from zeolite X. Scale bar is 1 μm. Reprinted with permission.⁵ Copyright 2012 Elsevier.

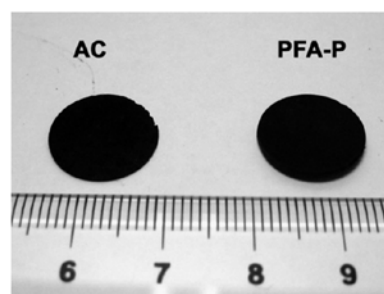


Fig. 17 Photographs of pelletized activated carbon (AC) and ZTC (PFA-P) pressed at 573 K and 147 MPa without binder. Reprinted with permission.¹⁵⁹ Copyright 2007 Elsevier.

In MOFs, crystallographic density is used to calculate ρ_{max} .²⁵⁵ In non-crystalline materials including ZTCs, ρ_{max} can be calculated by the following equation:

$$\rho_{\text{max}} = \frac{1}{\rho_{\text{true}}^{-1} + V_{\text{total}}} \quad (3)$$

where V_{total} [$\text{cm}^3 \text{g}^{-1}$] is a total pore volume determined by gas adsorption measurement, e.g. N_2 adsorption, on the pelletized sample, and ρ_{true} [g cm^{-3}] is a true density of pellet excluding its pore volume as well as any spaces inside the pellet. Note that V_{total} can include only the volume of pores which are less than ca. 100 nm. If the porous material includes large macropores ($> 100 \text{ nm}$), V_{total} underestimates the pore volume, resulting in the overestimation of ρ_{max} . However, Type-I ZTC is intrinsically microporous, and other types of ZTCs are usually not macroporous, too. Thus, the equation (3) works well for ZTCs. The value of ρ_{true} can be practically determined as a He density, and the ρ_{true} of ZTC has been reported to be 1.5–1.9 g cm^{-3} .^{23, 64} ρ_{max} is actually an apparent density of a ZTC particle having the properties of ρ_{true} and V_{total} . If ZTC particles are compacted to be pellet without any additional inter-particle spaces, the density of pellet becomes ρ_{max} . In other words, ρ_{max} is the upper limit of the packing density. Actual pellets contain some

amount of inter-particle spaces which are too large to be evaluated by N₂ physisorption, and therefore, the actual ρ of pellets always becomes smaller than ρ_{\max} . Thus, S_v has to be smaller than $S_{v-\max}$. As found from Table 5, the reported ρ and S_v exceed the theoretical upper limits (ρ_{\max} and $S_{v-\max}$), and it is found that they are overestimated. This is apparently caused by the underestimation of the pellet volume. One probable reason for this underestimation is the remarkable flexibility of ZTC (see 4.2).¹⁸³ If the pellet volume is measured under loading force, the volume can be smaller than that at a force-free condition. The actual S_v values achieved by ZTC pelletization seem to be at most $\sim 1200 \text{ m}^2 \text{ cm}^{-3}$.

Table 5 Properties of pelletized ZTCs.

S_{BET} ($\text{m}^2 \text{ g}^{-1}$)	ρ^a (g cm^{-3})	S_v^a ($\text{m}^2 \text{ cm}^{-3}$)	ρ_{\max}^b (g cm^{-3})	V_{total}^c ($\text{cm}^3 \text{ g}^{-1}$)	$S_{v-\max}$ ($\text{m}^2 \text{ cm}^{-3}$)	Ref.
1500	0.89	1340	0.78	0.76 ^d	1166	159
932	0.98	913	1.08 ^e	0.40 ^f	1006	171
2038	0.82	1671	0.53	1.22	1080	64
1897	0.88	1670	0.51	1.29	970	64

^a Reported values in literature. ^b Calculated by the equation (3). ^c Calculated from the N₂ adsorption (77 K) amount at $P/P_0 = 0.99$. ^d Read from the N₂ isotherm data. ^e Obtained by using $\rho_{\text{true}} = 1.9 \text{ g cm}^{-3}$, because the value is not given. ^f Since V_{total} was not reported, a micropore volume is used instead. Therefore, $S_{v-\max}$ is underestimated.

4.8 Synthesis of other materials by using ZTC

ZTCs or their precursors (carbon/zeolite composites) are useful also for the synthesis of other functional materials. Schlienger *et al.* synthesized boron nitride-based porous materials by using ZTC as a template.²⁵⁶ Though the ordered structure was lost, the resulting materials exhibited a high S_{BET} ($570 \text{ m}^2 \text{ g}^{-1}$).²⁵⁶ Asgarian *et al.* reacted ZTC with boron oxide and magnesium to prepare nanostructured boron carbide.²²¹ Moreover, Nourbakhsh^{224, 257} and Shcherban *et al.*²⁵⁸ converted carbon/zeolite composites into silicon carbides.

5. Applications of ZTC

ZTCs have been used for a variety of applications. The relevant literature is summarized in this chapter. For each application, introductory statements are provided for the minimal necessary background to help readers to grasp the significance of ZTCs in the individual field.

5.1 Adsorbents

Type-I or II ZTCs have been examined for removal of monoaromatic compounds^{165, 169} and pharmaceutical antibiotics.¹⁶⁷ Compared to microporous activated carbons, ZTCs exhibit faster adsorption/desorption kinetics and a larger normalized adsorption amount per surface area because of their three-dimensional ordered pore network and good pore accessibility.¹⁶⁵ The adsorption properties of Type-III ZTCs have been also examined,^{153, 213, 235, 237} whereas their advantages are not very much clear because of the random pore structures similar to those of activated

carbons. For bulky applications, e.g. water treatment, a large amount of adsorbent is required with a very low material price. Rather than such purposes, ZTCs would be advantageous for more specific applications in which ZTCs are distinguished from other adsorbents regarding to their ordered pore network and/or uniform pore size.

5.2 Hydrogen storage

From the developed microporosity of ZTCs, physisorption-based hydrogen storage has been investigated by many researchers.¹²⁻⁷⁰ The detailed background of hydrogen storage in nanoporous materials can be found in some excellent review papers.²⁵⁹⁻²⁶¹

5.2.1 Measurement and data analysis

Before mentioning the relevant literature, it is important to know the background of measurement techniques and data analysis as well as interpretation. There are two major measurement techniques, gravimetric and volumetric using a microbalance and a Sieverts apparatus, respectively. For the measurement below 1 bar of hydrogen pressure, conventional volumetric adsorption apparatuses (Sieverts type) have been commonly used. For high-pressure examination, both gravimetric and volumetric methods are found in literature, while the Japanese Standards Association has adopted the volumetric method (JIS H 7201) from its accuracy and reliability. Temperature has a great impact on the physisorption amount, and hydrogen storage data have been reported mainly in the following two temperature regions: liquid-nitrogen temperature (77 K) and ambient temperature (273-353 K). Cryogenic hydrogen storage at 77 K is potentially expected for mass-transfer of hydrogen, for example transportation for hydrogen stations, which is presently done by liquid hydrogen trailers. On the other hand, hydrogen storage around ambient temperature is required for ubiquitous applications including fuel cell vehicles (FCVs).²⁶² In both temperatures, a large storage amount is achieved in high-pressure range, and therefore, the high-pressure data are highlighted here.

A particular attention has to be paid to the two different expressions of hydrogen storage amount: surface excess amount (M_{ex} [$\text{g-H}_2 \text{ g}^{-1}$]) and total storage amount (M_{total} [$\text{g-H}_2 \text{ g}^{-1}$]). The former is the net increase from bulk hydrogen-gas concentration by the interaction with adsorbent. The surface excess amount is measured experimentally. The total storage amount is the sum of M_{ex} and hydrogen gas existing in the pore of the material without interaction, and is expressed by the following equation.

$$M_{\text{total}} = M_{\text{ex}} + \rho_{\text{H}_2} V_{\text{total}} \quad (4)$$

where ρ_{H_2} [$\text{g-H}_2 \text{ cm}^{-3}$] and V_{total} [$\text{cm}^3 \text{ g}^{-1}$] are density of bulk hydrogen gas and total pore volume of the porous material, respectively. Thus, M_{total} is always larger than M_{ex} . In the previous literature for high-pressure hydrogen storage in ZTCs, the storage amount data were often shown without any description, often causing misunderstanding. For fundamental discussion on hydrogen adsorption associated with material properties, M_{ex} is more meaningful, and M_{total} is of importance for practical use.

5.2.2 Cryogenic hydrogen storage in ZTC

Table 6 High-pressure hydrogen storage data on ZTCs and reference materials.

Material ^a	ZTC type	A.C. ^b	S _{BET} (m ² g ⁻¹)	V _{total} (cm ³ g ⁻¹)	V _{micro} (cm ³ g ⁻¹)	T (K)	P (bar)	M.M. ^c	M _{total} ^d (wt%)	M _v ^e (g L ⁻¹)	M _{v-max} ^f (g L ⁻¹)	Q _{st} ^g (kJ mol ⁻¹)	Ref.
CB850h	I	N	3150	1.95	1.13	77	20	G	6.9		28 ^h	8.2	16
ZTC-3	I		3591	1.81	1.66	77	20	V	6.4		29	6.5	46
C10-ZTC-5	II		3041	1.41	0.91	77	20	G	7	50.4	36 ^h		56
CZ13XFAETP	I		3021	1.0	1.56	77	20	G	6.6	46	32 ^h		64
PCN-68 ⁱ			5109	2.13	1.75 ^j	77	20	V	8.4		35 ^k	6.09	268
TC	I		3400	1.5	1.2	298	100	V	1.9		10		17
P7(2)-H	I		3800	1.7	1.58	303	340	V	5.7		27	7.8	23
ZTC-3	I		3591	1.81	1.66	298	300	V	5.1		23	6.5	46
6wt%Pt on TC	I	Pt (6%)	2755	1.2	1.0	298	100	V	2.2		13	14	17
Ru/TC	III	Ru (6%)	3004	1.46		298	100	V	2.5		13	25	19
ZTC-750		LiBH ₄ (53%)	12	0.03		573	120	TPD	6.92	75.43			62
A3-12 ^l			988	0.49	0.56	298	100	V	1.0	7	11		266
Be-BTB ⁱ			4030	1.52	1.52 ^m	298	95	V	2.0		10 ^k	5.5	267
PCN-68 ⁱ			5109	2.13	1.75 ^j	298	100	V	2.7		10 ^k	6.09	268

^a Samples without annotation are ZTCs. ^b Additional component. The weight ratio is shown in parenthesis if it is provided in literature. ^c Measurement method. G, V, and TPD stand for gravimetric method, volumetric method, and temperature-programmed desorption, respectively. ^d Total storage amount based on material mass (gravimetric storage amount) at *T* and *P*, expressed by the unit of wt%. When only surface excess amount (*M_{ex}*) is given in literature, *M_{total}* is calculated by the equation (4). ^e Total storage amount based on material volume (volumetric storage amount) reported in literature. ^f Theoretical maximum of *M_v*, calculated by the equation (6). When ρ_{true} is not given in literature, the value of type-I ZTC (1.9 g cm³)²³ is used. ^g The maximum value of *Q_{st}* at minimal coverage. ^h Measured by the gravimetric method (see the discussion on Fig. 18). ⁱ MOFs. ^j Calculated from the total pore volume (experiment) and pore-size distribution. ^k Calculated by the same manner as that for ZTCs. ^l Activated carbon monolith. ^m Microporous crystal.

Fig. 18 shows *M_{ex}* of several different types of materials including ZTCs, measured at 77 K and 20 bar, plotted against micropore volume (*V_{micro}*) of the materials. The relation between material properties and cryogenic high-pressure hydrogen adsorption amount has been thoroughly investigated on ZTCs already,^{12, 16, 18, 22, 25, 27, 29, 31, 34-37, 42, 45, 46, 51-56, 58, 64, 67} and it has been revealed that *M_{ex}* depends on *V_{micro}* (or also roughly on *S_{BET}*) almost regardless of the type of ZTCs.^{37, 43, 58, 67} This is a common tendency also in other porous materials including activated carbons, zeolites, and MOFs.^{58, 259} Indeed, a good correlation can be seen in the data obtained by the volumetric method regardless of the type of material and the presence of metal in Fig. 18. Thus, ZTC with developed microporosity is advantageous for cryogenic hydrogen storage compared to mesoporous materials. On the other hand, the data obtained by the gravimetric method diverges upwards in Fig. 18, suggesting the tendency of overestimation and/or large measurement errors.

The van der Waals interactions of hydrogen molecules to adsorbents is very weak, and its noticeable enhancement by the chemical structure of adsorbents is unfortunately not expected even at cryogenic conditions, in porous carbon materials. Indeed, chemical functionalities like N-containing groups have been revealed to be not effective.²⁵ Though there have been some reports on enhanced hydrogen storage by Pt^{28, 35, 43} and Pd⁵¹ through the hydrogen spillover mechanism at 77 K, the occurrence of hydrogen spillover at such a low temperature seems to be actually difficult.^{17, 20} Spillover is a well-known phenomenon in porous materials doped with metal nanoparticles such as Ru, Pt, and Ni.¹⁹ H₂ molecules are dissociatively adsorbed on the metal surface (chemisorption), and atomic hydrogens (H radicals) migrate to the support materials. The migration step is called spillover.^{263, 264} At 77 K, however, chemisorption does not occur on Pt. Moreover,

the spillover-based storage amount is decreased with decreasing temperature,^{57, 265} and it is estimated to become negligible at 77 K. Indeed, Yang *et al.* reported no enhancement effect in ZTCs which were doped with many different kinds of metals.²⁰ As shown in 5.2.3, the effect of metal becomes effective around ambient temperature.

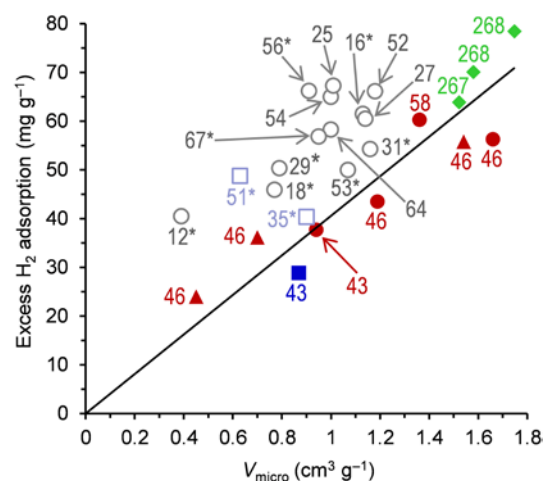


Fig. 18 Literature data on surface excess amounts (*M_{ex}*) of H₂ at 77 K and 20 bar, which are plotted against micropore volume (*V_{micro}*). Reference numbers are shown besides each plot. In the references associated with asterisk, only *M_{total}* is found, and therefore, *M_{ex}* is calculated by the equation (4). Blank and solid symbols are for the data measured by the gravimetric and volumetric methods, respectively. Circle, square, triangle, diamond symbols are for ZTCs, metal-doped ZTCs, activated carbons, and MOFs, respectively. An approximation line for the data obtained by the volumetric method is shown.

Representative hydrogen storage data on ZTCs are summarized in Table 6, together with that of a high-performance activated carbon monolith.²⁶⁶ For comparison, the data of the best MOFs are shown in Table 6, and also in Fig. 18 and 19.^{267, 268} The data of the best

MOFs were selected from review papers providing comprehensive catalogues of MOFs.^{259, 260} At 77 K, M_{total} is in the range of 6-7 wt% (0.064-0.075 g g⁻¹) in ZTCs. These values are comparably high to those of other highly porous carbon materials,⁵⁶ but not as high as that of the best MOF.

For practical application, not only M_{total} , but also the storage amount based on the material volume (M_V [g-H₂ cm⁻³]) is important to reduce the volume of the storage media. M_V is calculated by the following equation:

$$M_V = M_{\text{total}} \rho \quad (5)$$

As mentioned at the equation (1), ρ [g cm⁻³] is a pellet density for a pelletized sample, or a tap density for a powdery sample. Instead, by using the theoretical maximum density (ρ_{max}) obtained by the equation (3), the theoretical maximum M_V ($M_{V-\text{max}}$ [g-H₂ cm⁻³]) can be calculated as follows:

$$M_{V-\text{max}} = M_{\text{total}} \rho_{\text{max}} \quad (6)$$

$M_{V-\text{max}}$ is the upper limit of M_V .

Though very high M_V values (50.6 and 40 g L⁻¹) have been reported at cryogenic conditions,^{56, 64} they exceed the corresponding $M_{V-\text{max}}$ (39 and 34 g L⁻¹, respectively), most probably because of the reason described in 4.7. The actual achievable values in ZTCs would be in the range of 30-40 g L⁻¹ (Table 6). Nevertheless, $M_{V-\text{max}}$ of ZTC is more catching up to those of MOFs, compared to M_{ex} . This is probably because of the graphene-based framework. In-plane carbon-atom density of graphene is high, and the occupied volume by graphene-based framework becomes relatively small, compared to MOFs. Moreover, porous carbons have advantages of superior thermal stability, chemical stability, hydrophobicity, and mechanical strength, over MOFs. Thus, ZTC is still one of the promising candidates for cryogenic hydrogen storage.

The isosteric heat (Q_{st}) of adsorption in ZTCs at the lowest coverage state is in the range of 6-9 kJ mol⁻¹,^{12, 29, 46} almost the same as those in activated carbons²³ and MOFs.²⁵⁹

5.2.3 Hydrogen storage around ambient temperature in ZTC

Around ambient temperature, M_{ex} correlates well with specific surface area, regardless of the type of material and N-doping.^{23, 46, 48, 58} Fig. 19 shows M_{ex} measured at 298-303 K at 100 bar versus S_{BET} . Indeed, the data on ZTCs, activated carbons, and MOFs display a good correlation with S_{BET} . Similar to the case of cryogenic conditions, ZTCs are advantageous in volumetric capacity rather than gravimetric over MOFs (Table 6). Moreover, porous carbons can be molded into high-density pellets,²⁶⁶ and this is very important for practical application. Under high pressure, ZTCs with high surface areas exhibit M_{total} up to 5.7 wt% even at ambient temperature (Table 6), yielding $M_{V-\text{max}}$ of 27 g L⁻¹. These values are very competitive to those of the best MOFs, and approaches the US Department of Energy (DOE) target for 2020: 4.3 wt%-H₂ in a system and 30 g-H₂ L⁻¹-system at an operating temperature range of 233-333 K, but still much less than the corresponding ultimate target: 6.1 wt%-H₂ and 50 g-H₂ L⁻¹-system.²⁶² To further enhance hydrogen storage at ambient temperature, spillover-assisted hydrogen storage has been expected. As is found from the data on TC and Ru/TC in Table 6, doping Ru nanoparticles greatly enhances the storage amount, together with a noticeable increase of Q_{st} .

Indeed, in Fig. 19, metal-doped ZTCs are significantly deviated from the physisorption-based line. However, the remarkable enhancement effect by metal doping on ZTCs has been reported only by Yang's group up to date,^{17, 19, 26, 33, 48} and no one including us (see the datum #51 in Fig. 19) can reproduce similar results.²³ Additionally, the data above 100 bar have not been reported. It is actually not easy to obtain sufficient reproducibility in hydrogen uptake measurement on metal-doped samples. As Ghimbeu *et al.* pointed out, the presence of surface oxide layers on metal particles often inhibits precise measurement.³⁸ We have developed a reliable protocol for the measurement at a low-pressure range (< 1 bar), and confirmed reproducible spillover storage, which is enhanced with increasing temperature in Pt-loaded ZTCs.⁵⁷ However, there are still difficulties in high-pressure measurement on metal-doped ZTCs, and further effort is necessary to develop a reliable protocol of material preparation as well as analysis. Only based on such a reliable protocol, promising materials could be fabricated.

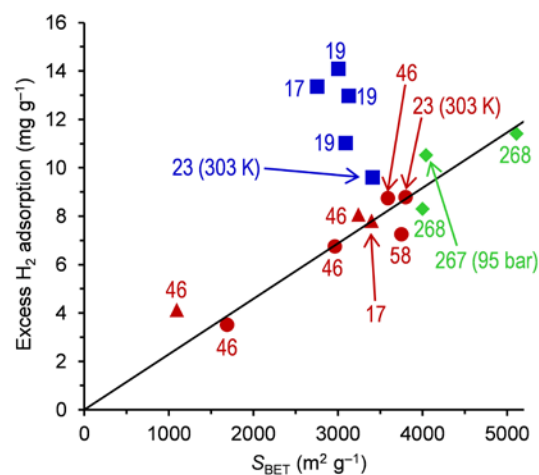


Fig. 19 Literature data on surface excess amounts of H₂ (M_{ex}) at 298 K and 100 bar, which are plotted against BET surface area (S_{BET}). Reference numbers are shown besides each plot. All the data are measured by the volumetric method. Circle, square, triangle, and diamond symbols are for ZTCs, metal-doped ZTCs, activated carbons, and MOFs, respectively. Measurement conditions are shown in parenthesis, when they are different from 298 K and 100 bar. An approximation line is calculated with excluding the data of metal-doped ZTCs.

5.2.4 Hydride/ZTC composites

Jie *et al.* introduced LiBH₄ in ZTC, and the resulting composite exhibit high M_{total} and M_V (Table 6).⁶² By the nano-confining effect, the composite can release hydrogen at 467 K, 181 K lower than the case of bulk LiBH₄. Such a strategy may be further developed to reduce the uptake/release temperature down to the target range (233-333 K) for on-board hydrogen storage.

5.3 Methane storage

Methane storage has been also investigated in ZTCs,^{63, 163, 166, 171, 187, 198, 199, 240, 255, 269-272} aiming to evaluate their potential for natural gas storage towards vehicle applications. General background of methane storage in nanoporous materials has been summarized in previous review papers,^{255, 269-273} and we focus on the performance of ZTCs here. For methane storage, a volumetric total storage amount ($M_{V/V}$) is popularly expressed by the unit of cm³ (STP) cm⁻³ (equivalent volume of methane at the standard temperature and

pressure: $T = 273.15$ K, $P = 1$ atm, divided by the volume of the adsorbent material). $M_{V/V}$ is obtained by the following equation:

$$M_{V/V} = 11.1 \times M_V \quad (7)$$

Besides, the maximum $M_{V/V}$ ($M_{V/V-\max}$) can be calculated by the equation (7) using $M_{V-\max}$ instead of M_V . Practically, the deliverable capacity (M_{del}) is of importance and it can be obtained by subtracting the amount of methane remaining at the depletion pressure from the amount of methane stored per volume of material in a fully loaded state. The Advanced Research Projects Agency-energy (ARPA-E) of DOE sets a target of $315 \text{ cm}^3 \text{ cm}^{-3}$ at ambient temperature with a storage pressure of 65 bar and a depletion pressure of 5.8 bar.²⁷³ Thus, the maximum deliverable capacity ($M_{\text{del-max}}$) is calculated by the following equation.

$$M_{\text{del-max}} = M_{V/V-\max}(@65 \text{ bar}) - M_{V/V-\max}(@5.8 \text{ bar}) \quad (8)$$

Stadie *et al.* reported the methane storage in Type-I ZTC with a high-surface area (ZTC-3 in Table 6) at 298 K up to 100 bar, and found unusual increase of Q_{st} with increasing methane uptake, which could be advantageous for large uptake.¹⁸⁷ Nevertheless, $M_{\text{del-max}}$ is $125 \text{ cm}^3 \text{ cm}^{-3}$, far less than the ARPA-E target. Simon *et al.* performed a systematic survey of methane uptake in over 650,000 materials by using computer simulation, and found that $M_{\text{del-max}}$ of the best material is ca. $200 \text{ cm}^3 \text{ cm}^{-3}$, unfortunately still less than the target. The similar values have been indeed reported in several types of MOFs.²⁷⁴⁻²⁷⁷ Considering the large gap between the capacities of ZTC (up to $125 \text{ cm}^3 \text{ cm}^{-3}$) and the best MOFs and the systematic material survey (ca. $200 \text{ cm}^3 \text{ cm}^{-3}$), it seems to be difficult to achieve a fascinating performance in ZTCs.

5.4 CO₂ capture

Towards saving the earth from its warming, the reduction of CO₂ emission is a very important issue in the world. Physisorption-based CO₂ capture in nanoporous materials has been one of the promising options for industry.^{271, 278-280} There are three major methods for CO₂ capture: post-combustion, pre-combustion, and oxy-fuel combustion.²⁷⁸ The former two methods especially have room for

improvement of the efficiency by using nanoporous materials.

In the post-combustion, CO₂ is separated from the mixture gas generated by combustion. The gas composition (volume ratio) is as follows: 73-77% N₂, 15-16% CO₂, 5-7% H₂O, 3-4% O₂, and minor components (< 1%) such as SO₂, SO₃, NO_x, HCl, CO, hydrocarbons, and Hg.²⁷⁸ Thus, highly-selective adsorption of CO₂ in the gas mixture around ambient temperature and pressure is required. The post-combustion has been the most explored strategy to date because it is easily installed to the existing factories and power plants.

The pre-combustion aims to separate pure H₂ fuel gas from coal-derived shifted synthesis gas (called shifted syn gas) containing ca. 70-80% H₂, 15-25% CO₂, 1-3% CO, and 3-6% CH₄.²⁷⁸ While the post-combustion needs a temperature or vacuum swing-based process, the pre-combustion can be operated by a pressure-swing process above atmospheric pressure because the shifted syn gas is produced at a high pressure. Thus, the desorption (regeneration) of CO₂ from sorbent is much easier than that of the post-combustion.

For both methods, adsorbents have to satisfy the several requirements such as high CO₂ uptake, high CO₂ selectivity, good cyclability, fast kinetics, stability against water vapor and acidic gases, and inexpensive material cost.

Table 7 summarises the representative data on the CO₂ capture in ZTCs together with high-performance activated carbons²⁸¹ at low and high pressure regions, applicable for the post-combustion and the pre-combustion, respectively. For comparison, the data of the best MOFs²⁸²⁻²⁸⁴ are also shown, which were selected from the comprehensive review paper.²⁷⁸ The performance of nanoporous materials for the post-combustion can be roughly evaluated by single-component adsorption isotherms of CO₂ and N₂ at ambient temperature and pressure. By using the amounts of CO₂ uptake (q_{CO_2} [mmol g⁻¹]) and N₂ uptake (q_{N_2} [mmol g⁻¹]) at their partial pressures (P_{CO_2} and P_{N_2}) in the target gas mixture, the selectivity of CO₂ to N₂ (S) can be calculated as follows:

Table 7 A list of ZTCs examined for CO₂ capture.

Material ^a	ZTC type	A.C. ^b	S_{BET} (m ² g ⁻¹)	V_{total} (cm ³ g ⁻¹)	V_{micro} (cm ³ g ⁻¹)	T (K)	P (bar)	M_{total} ^c (wt%)	Selectivity CO ₂ /N ₂	Q_{st} ^d (kJ mol ⁻¹)	Ref.
CEMFAFE			3698	1.88	1.14	298	0.15	3.0		32	142
CEM750		N (4.7%)	3360	1.71	1.24	298	0.15	4.1	13 ^e	36	142
TC-EMC			3840	1.8		298	0.15	3.4	1.3 ^e	30	145
N-TC-EMC		N (7% ^f)	2559	1.4		298	0.15	6.5	6.1 ^e	56	145
AS-2-600 ^g			1260	0.62	0.55	298	0.15	5.0			281
Mg ₂ (dobdc) ^h			1800	0.73	0.73 ⁱ	313	0.15	20	55	42	283
mmen-Cu-BTTri ^h			870	0.36	0.36 ⁱ	298	0.15	9.5	165 ^e	96	284
FA+Ac-873/973-4/1	I		3213	1.6	1.4	298	25	53			166
EMT-ZTC	I		3420	1.69	1.47	298	32	53			141
ZTC_1000	II		3010	1.84	1.22	298	40	54 ^j			173
MOF-200 ^h			4530	3.59		298	40	72			282

^a Samples without annotation are ZTCs. ^b Additional component. The weight ratio is shown in parenthesis. ^c Total storage amount based on material mass (gravimetric storage amount) at T and P , expressed by the unit of wt%. When only surface excess amount (M_{ex}) is given in literature, M_{total} is calculated by the equation (4). ^d The maximum value of Q_{st} at minimal coverage. ^e Calculated by the adsorption isotherm (excess amount). ^f Measured by XPS. ^g Activated carbon. ^h MOFs. ⁱ Microporous crystal. ^j It is not clear where the reported value is excess amount or total amount. By assuming it as the former, a total storage amount is calculated.

$$S = \frac{q_{\text{CO}_2}/q_{\text{N}_2}}{P_{\text{CO}_2}/P_{\text{N}_2}} \quad (9)$$

P_{CO_2} and P_{N_2} are often selected as 0.15 and 0.75 bar, respectively.²⁷⁸ Though the Ideal Adsorbed Solution Theory (IAST) provides more reliable selectivity, S is still useful for a quick grasp of a tendency, and it is easy to compare the data in literature.

Compared to the cases of H_2 or CH_4 , the tuning of pore size is of great significance in CO_2 uptake. The appropriate pore size for efficient CO_2 uptake is in the range of 0.3–0.4 nm,²⁸⁰ and narrow micropores below 0.35 nm are effective to achieve high selectivities for CO_2 over N_2 and CO_2 over CH_4 .²⁷⁸ Moreover, polar functional groups do enhance the CO_2 uptake because of its higher polarizability and quadrupole moment than those of N_2 . Indeed, Xia *et al.*¹⁴² and Wang *et al.*¹⁴⁵ have reported the noticeable enhancement of CO_2 uptake along with the increase of Q_{st} by N-doping into ZTCs (Table 7), and N-doped ZTC exhibits better CO_2 uptake than that of high-performance activated carbon. Nevertheless, CO_2 uptake as well as selectivity is far less than those of the best MOFs at 0.15 bar. As is found from their data (Table 7), high porosity is not directly related to the performance. Much more important is the tuning of pore size and introduction of polar groups. As mentioned earlier, a precise pore-size control is possible by hot-pressing in ZTCs, and the introduction of polar groups is also possible by a variety of methods. Thus, there might still be room to improve the CO_2 uptake in ZTCs.

At a high-pressure region, developed microporosity is of importance for a high CO_2 uptake, and MOFs seem to be superior to ZTCs (Table 7).

5.5 Electrochemical capacitors

ZTCs have been intensively investigated about their potential of electrode materials for electrochemical capacitors (also called supercapacitors or ultracapacitors), from their sufficient electric conductivity and excellent microporosity.^{25, 71–95}

5.5.1 Background of electrochemical capacitors

In electrochemical capacitors, capacitance (C [F g^{-1}]) is the amount of charge which is stored in a pair of two electrodes, basically through the formation of electric double-layer at the interface of the electrode and an electrolyte. Therefore, C in principle depends on the surface area of electrodes. However, there are several factors which modulate this relation through both negative and positive effects. The negative effect occurs through the following reasons: (N1) poor wettability by an electrolyte; (N2) inner resistance of a carbon electrode; (N3) limitation of ion diffusion in narrow pores; and (N4) inhibition of ion invasion in very narrow pores. On the other hand, the positive effect occurs by: (P1) pseudocapacitance; and (P2) shortening of electrode-ion distance through de-solvation in very narrow pores. Among the negative and positive enhancements, (N3) and (P2) are conflicting. At a low current, the capacitance can be increased by (P2), whereas the (N3) effect becomes dominant at a high current.

It should be noted that the capacitor performance significantly varies depending on the measurement method or conditions. For example, the amount of active material, type of cell (two or three electrodes), electrolyte, potential (or voltage) range, and charge/discharge rate. Note that potential and voltage are different.

Hereafter, 'potential' is used when an energy level can be defined by a reference, while 'voltage' is used to express the potential difference between two electrodes. The method to calculate capacitance significantly affects the results, too. The value of C can be calculated from cyclic voltammetry (CV), electrochemical impedance spectroscopy (EIS), and galvanostatic discharge curves (GDC). Among them, GDC is generally considered as the most reliable method.²⁹ Thus, it is not easy to simply compare the reported capacitance values which are measured by using different techniques. Furthermore details about the background of the electrochemical capacitors can be found in some excellent review papers.^{285–287}

While C is measured by a two-electrode cell, a three-electrode cell provides single-electrode capacitance (C_{single}). C_{single} has the following relation with C measured by the corresponding symmetrical two-electrode cell.

$$C_{\text{single}} = 4C \quad (10)$$

Many authors prefer to express capacitance by C_{single} even if it is measured with a two-electrode cell, by using the equation (10). The equation (10) works as far as each electrode in a two-electrode cell functions symmetrically in a voltage range applied. However, the electrochemical behaviour is actually very asymmetric in Type-I and some of Type-II ZTCs, which consist mainly of ordered framework of single-layer graphenes. On the other hand, the behaviour of Type-III ZTCs is almost the same as those of activated carbons, and some of them can work symmetrically. The aforementioned background has often caused misunderstanding on the electrochemical property of Type-I ZTCs, which shows very unique behaviour as shown below.

5.5.2 Aqueous electrolytes

Type-I ZTC with a high surface area (ca. $3800 \text{ m}^2 \text{ g}^{-1}$) shows relatively low specific capacitance per surface area. This is because some segments of the ZTC framework are very narrow like graphene nano-ribbons, and show semiconductive nature.^{91, 94} Nevertheless, the capacitance can be remarkably enhanced by *in situ* introduction of electrochemically active functional groups as described below. Unlike Type-III or some of Type-II with relatively low ordered structure, Type-I and some Type-II ZTCs contain very active edge sites compared to activated carbons, probably because of the unique curved nanographene framework (Fig. 4). In aqueous electrolytes, they are easily oxidized as relatively low anodic potential (Fig. 12).¹⁸¹ As shown in Fig. 20, Type-I ZTC is intensively oxidized at the first anodic scan in 1M H_2SO_4 . The chemical structure change of ZTC is illustrated in Fig. 21. ZTC (Fig. 21a) originally contains some amount of oxygen-functional groups. By the anodic oxidation, a large amount of oxygen-functional groups are introduced on the edge sites rather than basal plane.⁸⁴ Interestingly, a large amount of quinone-type groups can be introduced unlike the case of chemical oxidation (Fig. 21b), thereby showing a large pseudocapacitance around 0.28 V (vs. Ag/AgCl) in the following cycles (Fig. 20). The capacitance measured by GDC achieves 300–500 F g^{-1} , because of the reversible quinone-hydroquinone redox reactions (Fig. 20b,c).⁸⁴

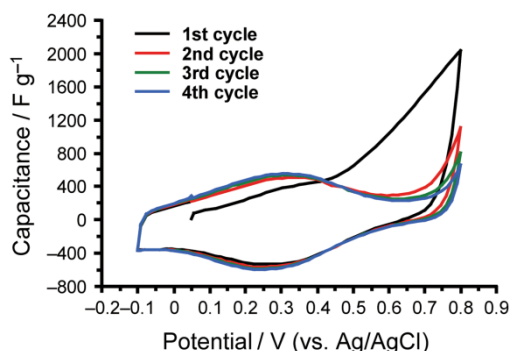


Fig. 20 CV patterns of Type-I ZTC measured with a three-electrode cell at 298 K in 1M H_2SO_4 . Scan rate is 1 mV s^{-1} . Reprinted with permission.⁸⁴ Copyright 2014 The Chemical Society of Japan.

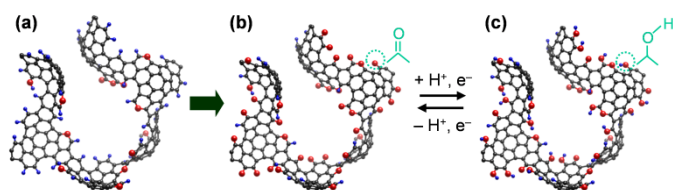


Fig. 21 Illustration for the structure change of Type-I ZTC upon electrochemical oxidation and the following redox reaction in an acidic electrolyte. (a) An enlarged structure model of ZTC. Black, blue, and red colours correspond to carbon, hydrogen, and oxygen atoms, respectively. ZTC originally has some oxygen-containing groups. (b) Quinone-functionalized ZTC prepared using electrochemical oxidation. (c) Reprinted with permission.⁸⁴ Copyright 2014 The Chemical Society of Japan.

While ZTC exhibits a promising performance in the positive potential range in an acid electrolyte, its capacitance is much lower in the negative potential range because of the lack of the pseudocapacitance, and moreover, a stable potential range of Type-I ZTC is limited to ca. -0.5 V (vs. Ag/AgCl) at a negative-electrode side.⁸⁶ Therefore, a symmetric capacitor using Type-I ZTC cannot exhibit a high energy density (E [Wh kg^{-1}]),⁸⁶ which is calculated by using C as follows.

$$E_j = \frac{1}{2} CV^2 \quad (11)$$

$$E = \frac{E_j}{3.6} \quad (12)$$

where E_j is energy with a unit of J g^{-1} , and V [V] is the range of applied voltage. To achieve a high energy density, capacitance should be high at both electrodes, and more importantly, the voltage range should be wide as much as possible.

In order to efficiently utilize the advantage of ZTC, we assembled an asymmetric capacitor using ZTC together with a high capacitance porous carbon, which is KOH-activated carbon ($S_{\text{BET}} = 2600 \text{ m}^2 \text{ g}^{-1}$) derived from a Spanish anthracite and possess a wider potential window at the negative-electrode side.⁸⁶ Such a configuration can exhibit a high energy density of 24.5 Wh kg^{-1} , which is comparable to those of conventional capacitors utilizing an organic electrolyte.

5.5.3 Organic electrolytes

In an organic electrolyte, Type-I ZTC shows similar but slightly different behaviour. Fig. 22 shows CV patterns of Type-I ZTC measured in 1M $\text{Et}_4\text{NBF}_4/\text{propylene carbonate}$ (PC). In the potential range of -1.5 to 1.0 V (vs. Ag/AgClO_4), ZTC is intensively oxidized above 0.5 V at the first anodic scan. It has been revealed that

oxygen-functional groups are introduced by this anodic oxidation through the analyses with temperature-programmed desorption, FT-IR, and XPS, and that PC is an oxygen source.⁸⁹ By the electrochemical oxidation, ZTC becomes to exhibit a large pseudocapacitance at two potential regions (a possible mechanism is shown in Fig. 23).⁸⁹ A similar behaviour can be seen also in another organic electrolyte: 1M LiPF_6 in ethylene carbonate (EC) and diethyl carbonate (DEC) (EC:DEC = 1:1), which is commonly used for lithium-ion batteries (LIBs) and lithium-ion capacitors (LICs). Thus, ZTC can exhibit a large pseudocapacitance in several different organic electrolytes.

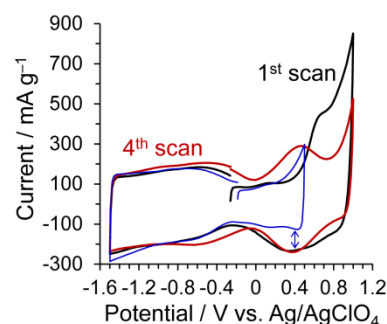


Fig. 22 CV patterns of Type-I ZTC measured with a three-electrode cell at 298 K in 1M $\text{Et}_4\text{NBF}_4/\text{PC}$. Scan rate is 1 mV s^{-1} . Two potential ranges are used: between -1.5 to 0.5 V (1^{st} cycle), and -1.5 to 1.0 V (1^{st} and 4^{th} cycle). Reprinted with permission.⁸⁹ Copyright 2015 Elsevier.

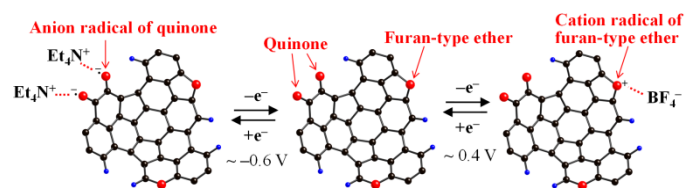


Fig. 23 A possible redox-reaction scheme of oxygen-functionalized ZTC in 1M $\text{Et}_4\text{NBF}_4/\text{PC}$. Reprinted with permission.⁸⁹ Copyright 2015 Elsevier.

Another advantage of ZTC is the compatibility of a high apparent density (ρ_{max}) and a high rate capability. It is well known that mesopores and macropores can greatly accelerate ion diffusion to achieve a high rate performance, but micropores ($< 2 \text{ nm}$) are inferior. Thus, there have been many publications on the development of “hierarchical” porous carbons with micropores and meso- and/or macropores. However, the presence of mesopores and especially macropores terribly lowers ρ_{max} , giving rise to a quite low volumetric capacitance ($C_{\text{single-V}}$ [F cm^{-3}]). The ordered pore-arrangement of ZTC enables a high rate capability despite the small pore size of 1.2 nm . Moreover, ρ_{max} of ZTC is much higher than those of the hierarchical carbons.⁷⁷ Thus, ZTC achieves a high $C_{\text{single-V}}$ of 89 F cm^{-3} , together with a good capacitance retention up to a high current.⁷⁷

To utilize its high pseudocapacitance, ZTC might be applied to a high-capacitance positive-electrode for LICs, in which the positive electrode works in a relatively narrow potential range within about $\pm 1 \text{ V}$ from an open circuit potential.

It is not advantageous for ZTC to be used for symmetric capacitors. A potential window of Type-I ZTC is ca. -2.0 to 1.0 V (vs. Ag/AgClO_4)

in 1M Et₄NBF₄/PC.⁸⁹ This means that its symmetric capacitor can stably work approximately only within 2.0 V, which is much less than the voltage of commercial capacitors (2.7 V). Thus, the improvement of anodic stability of ZTC is desired. The chemical modification of active edge sites is one of the possible ways for such improvement. For example, it has been reported that N-doping can improve the anodic stability of ZTC in aqueous electrolytes.^{71, 95}

As describe above, Type-I ZTC shows unique electrochemical properties. Its single-layer graphene framework provides a large surface area to achieve a high capacitance, while its large amount of active edge sites can be a double-edged sword with a high pseudocapacitance and a limited stability. To take only the advantage of high capacitance, it is desirable to construct a nanoporous framework by single-layer graphene which is free from edge sites. We have recently realized such a material called graphene mesosponge, and demonstrated that it has indeed exhibited an excellent anodic stability to achieve a high voltage charge/discharge up to 4 V in a symmetric cell.¹²⁷

5.5.4 Potential window of ZTC

Potential windows of Type-I ZTC^{84, 86, 89} in several electrolytes are summarized in Table 8. In addition to the data reported in literature, we show the results in 1 M LiPF₆ in a mixture of ethylene carbonate (EC) and diethyl carbonate (DEC) (1:1 by volume) in Fig. 24. As described above, in most of cases, ZTC is oxidized at the first anodic scan, and becomes stable in the potential range shown in Table 8. Note that the potential window can be actually changed depending on several factors, such as the quality and property of ZTC, N-doping^{71, 95} or other chemical modification, the construction of an electrochemical cell, and temperature. Nevertheless, Table 8 can be useful for a rough approximation. For electrochemical applications of ZTC, it is a matter of first priority to confirm the applicable potential range.

Table 8 Potential windows of Type-I ZTC in several electrolytes at 298 K.

Electrolyte	Potential window
1M H ₂ SO ₄	-0.5 to 0.8 V (vs. Ag/AgCl) ^{84, 86}
KOH	not stable ^a
1M Et ₄ NBF ₄ /PC	-2.0 to 1.0 V (vs. Ag/AgClO ₄) ⁸⁹
1M LiPF ₆ /EC+DEC(1:1)	1.2 to 4.7 V (vs. Li/Li ⁺) ^b
AlCl ₃ /[EMIm]Cl ^c	0.01 to 2.2 V (vs. Al/Al ³⁺) ²⁰⁷

^aType-I ZTC is not stable in a basic solution including a KOH electrolyte. When ZTC is immersed in strong base, it is gradually decomposed. ^bSee Fig. 24. ^c1:1 molar mixing ratio. [EMIm]Cl stands for 1-ethyl-3-methylimidazolium chloride.

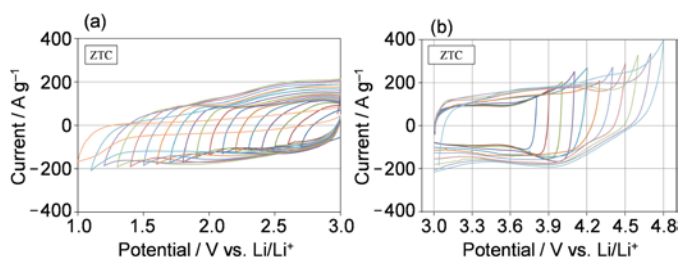


Fig. 24 CV patterns of Type-I ZTC (the same grade as that in ref. [89]) in (a) negative and (b) positive potential ranges. An electrode sheet (ZTC:CB:PTFE = 8:1:1) was cut out as a circular shape (ϕ 12 mm), and it was sandwiched by two circular SUS304 meshes (ϕ 16 mm), and used as a working electrode. Other setting for a three-electrode cell was the

same as those reported elsewhere.²⁸⁸ Scan rate is 1 mV s⁻¹. (a) and (b) were carried out by two separated cells. The measurement was started in the narrowest potential range, followed by the potential expansion by 0.1 V to negative (a) and positive (b) potential directions. At each potential range, CV was repeated four times. Only the 1st scan results at each potential range are shown here. In (a), capacitance decrease becomes evident below 1.1 V, while anodic current becomes intense at 4.8 V in (b). Thus, the stable potential window of ZTC is between 1.2 to 4.7 V (vs. Li/Li⁺) in 1M LiPF₆/EC+DEC.

5.6 Batteries

5.6.1 Lithium-ion batteries

There have been some reports on the anode properties of ZTCs for LIBs.^{135, 185, 193} The potential range of an anode is usually between 0.01 to 1.5 V (vs. Li/Li⁺) in 1M LiPF₆/EC+DEC, exceeding the stable range of ZTC (Table 8). Fortunately, at the first negative-direction polarization, the electrolyte is decomposed to form an ion-conductive layer called solid-electrolyte interface (SEI), which stabilizes the carbon framework. Thus, ZTCs exhibit a high reversible capacity over 1000 mAh g⁻¹. However, there are two serious problems:

(1) A large irreversible capacity of ca. 700-1200 mAh g⁻¹, upon the formation of SEI. When assembling a full cell together with a cathode material such as LiCoO₂, the irreversible capacity consumes lithium existing inside the full cell. Therefore, it is necessary to supply the corresponding amount of lithium by increasing the amount of cathode material to compensate the lithium loss in the anode side. This significantly increases the total mass of the full cell, resulting in the decline of the energy density.

(2) Non-constant delithiation potential which distributes up to ca. 3.0 V (Li/Li⁺). This lowers the voltage of a full cell, resulting also in the decline of the energy density. In conventional graphite, the delithiation potential is constant at 0.1 V.

To use ZTC for LIB anodes, these two problems have to be solved; otherwise it is difficult to expect its significance over other high-performance candidates such as Si.²⁸⁹⁻²⁹¹

5.6.2 Aluminium batteries

Stadie *et al.* applied Type-I ZTC to a cathode of aluminium batteries using Al metal as an anode (Fig. 25) in AlCl₃/[EMIm]Cl.²⁰⁷ They have confirmed that ZTC is stable in the potential range of 0.01-2.2 V (vs. Al/Al³⁺) (Table 8), corresponding to 1.4 to 3.6 V (vs. Li/Li⁺). Like the case of LICs, the cathode charges electricity by physical adsorption forming electric double layer, and therefore, ZTC is superior to other high-surface activated carbons. Thus, the full cells exhibited both high energy density (up to 64 Wh kg⁻¹, 30 Wh L⁻¹) and power density (up to 290 W kg⁻¹, 93 W L⁻¹), with a good reversibility within the charging voltage of 2.2 V.

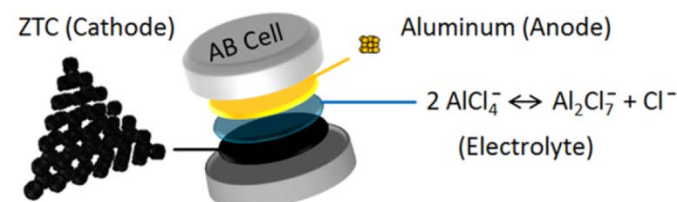


Fig. 25 Illustration of a full cell of the aluminium battery. Reprinted with permission.²⁰⁷ Copyright 2017 American Chemical Society.

5.6.3 Organic proton batteries

The developed porosity with relatively small pore size (ca. 1.2 nm) can be advantageous to stably immobilize active species which tends to be dissolved into an electrolyte. Nueangnoraj *et al.* used Type-I ZTC as hosts for two types of quinones, anthraquinone (for negative electrode) and tetrachlorohydroquinone (for positive electrode) for organic proton batteries. Their redox potentials are ca. -0.3 to -0.15 V (vs. Ag/AgCl) and 0.3 to 0.7 V, respectively, inside the potential window of ZTC in 1M H_2SO_4 (-0.5 to 0.8 V).^{84, 86} ZTC can accommodate these quinones up to ca. 60 wt% without forming crystalline solids (Fig. 26), while a high-surface activated carbon, Maxsorb[®], can ca. 50 wt%. The assembled device achieves an energy density of 30.6 Wh kg^{-1} which is superior to the activated-carbon-based capacitors working in the organic electrolytes and also to lead batteries.

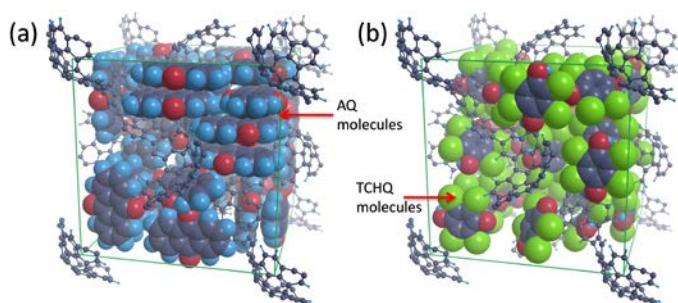


Fig. 26 A ZTC model stuffed with (a) 36 AQ molecules and (b) 31 TCHQ molecules. The dark-grey, blue, red, and green balls represent the carbon, hydrogen, oxygen, and chlorine atoms, respectively. Reprinted with permission.²⁰³ Copyright 2016 Elsevier.

5.6.4 Lithium-sulfur batteries

Cui *et al.* prepared ZTC with very small particle sizes (30-50 nm), and used them as a host of sulfur for cathodes of Li-S batteries. They expected better sulfur-carbon contact and polysulfide retention in a porous carbon host with ultrafine sizes. The ZTC nanoparticles were seemingly Type-III, though no XRD data were provided. The potential range of the cathode is 1.7 - 2.6 V (vs. Li/Li^+) in 1.0 M lithium bis(trifluoromethanesulfonyl)imide and 0.1 M LiNO_3 dissolved in $1,3$ -dioxolane and $1,2$ -dimethoxyethane ($1 : 1$, v/v). Though the stability data were not provided, the range of 1.7 - 2.6 V seems within a potential window on the analogy of the one in 1M $\text{LiPF}_6/\text{EC}+\text{DEC}$ (Table 8), and additionally, Type-III is generally more stable than Type-I despite its other inferior performances. ZTC was modified by amphiphilic N-polyvinylpyrrolidone (PVP) in advance, and the modified ZTC could accommodate 46 wt% of sulfur. The resulting composite exhibited the initial lithiation capacity of ca. 1240 mAh g^{-1} based on the sulfur mass (670 mAh g^{-1} based on the composite mass), and it became 880 mAh g^{-1} (475 mAh g^{-1} , composite-mass base) at the 50 cycle. Since the ZTC used was Type-III prepared by the simple impregnation-carbonization method, there would be still room to improve this system.

5.7 Fuel cells

Pt- or Pt-Ru loaded ZTCs have been tested as anodes for direct methanol fuel cells (DMFCs)^{154, 174, 192} and as cathodes for polymer electrolyte fuel cells (PEFCs),^{177, 188, 208, 209} and it is found that their performance is almost comparable to commercial Pt/C catalysts. In

most of cases, ZTCs were Type-III or Type-II with poor structure regularity, and therefore, the advantages of ZTC have been not very much evident compared to other nanoporous carbons. For practical applications, an anodic stability is of significance. This is important even for cathode of PEFC because the cathode side is actually subjected to severe oxidative environment upon the re-starting of the PEFC system from a rest state. Compared to other porous carbons and carbon blacks, ZTCs are inferior regarding the anodic stability because of their larger amount of edge sites.

Kwon *et al.* demonstrated that N-doped ZTC (Type-II) exhibits a better catalysis for ORR than N-doped reduced graphene oxides.¹³⁶ The activity of N-doped ZTC approaches that of a commercial Pt/C (Pt: 20 wt%) in a 0.1M KOH electrolyte. On the other hand, our group reported that the ORR activity of N-doped ZTC (Type-I) can be further improved by BN-doping.⁹⁴ However, its activity is not as high as that of a commercial Pt/C in an acidic electrolyte (0.1 M HClO_4). A further improvement is necessary for leading to the development of non-Pt catalysts for PEFC based on ZTC.

5.8 Catalysts

ZTCs have been investigated also as catalyst supports or catalysts.^{164, 178, 182, 189, 191, 194, 205, 215}

As a catalyst support, ZTC provides a large microporous space for accommodating catalyst nanoparticles. Moreover, the developed and uniform microporosity of ZTC is advantageous for fast mass transportation, large capacity of adsorption, and size-exclusion of large molecules. Donphai *et al.* loaded TiO_2 nanoparticles onto Type-I ZTC, and demonstrated a good photocatalysis of the resulting composite towards the degradation of organic contaminant.¹⁸⁹ Jiang *et al.* reported a high catalysis of Pt-loaded ZTC (Type-I) towards hydrogenation reaction.¹⁹¹ Choi *et al.* prepared S-doped ZTCs, and found that it can accommodate single Pt atoms (Fig. 13) to show selective reduction of O_2 into H_2O_2 .

It is also possible to use ZTCs or chemically-modified ZTCs directly as catalysts. Melo Freire *et al.* reported high activity of several types of N-doped templated carbons for Knoevenagel condensation.¹⁶⁴ However, the tested ZTC was poorly porous Type-III ($S_{\text{BET}} = 412 \text{ m}^2 \text{ g}^{-1}$), and therefore, the performance may be further improved. Fukuhara *et al.* reported a high activity of Type-II ZTC modified with $-\text{SO}_3\text{H}$ towards the hydrolysis of cellobiose and the Beckmann rearrangement.¹⁸² Fukuoka's group discovered a unique catalysis of Type-I ZTC towards the depolymerization of long-chain glucan.^{194, 205}

Considering the chemical-structure and the flexibility of a ZTC framework described in the chapter 4, there is a great possibility to develop new catalyst applications using ZTCs.

5.9 Solar evaporation

Wang *et al.* recently reported an application of ZTC towards solar evaporation,¹³⁷ which is one way of solar energy harvesting and expected as means of seawater desalination and wastewater treatment. Carbon materials have broadband absorption properties, and can efficiently absorb solar spectrum. While the relevant investigation has focused on crystalline carbons such as graphite, graphene, and carbon nanotubes so far without rational reasons, Wang *et al.* used ZTC as a low crystalline carbon material and

examined the relation between the property of ZTC and its performance. They used Type-II ZTC with relatively low surface area ($S_{\text{BET}} = 1704 \text{ m}^2 \text{ g}^{-1}$), whereas still found that ZTC exhibits a high energy conversion efficiency of 72%, thanks to a good wettability by the presence of a large amount of oxygen-functional groups. The performance might be further improved by applying high-quality Type-I ZTC.

6 Conclusions and Perspective

In this review article, the development and applications of ZTCs have been summarized over recent 20 years since the first synthesis in 1997. We have defined the three categories for ZTC quality, Type-I, II, and III (high to low), depending on the degree of ordered structure and inclusion of non-templated carbon portion. The Type-I ZTCs consist of a curved and single-layer narrow graphene framework, affording unique properties and advantages over other nanoporous carbon materials, while Type-III ZTCs are not greatly different from the conventional nanoporous carbons like activated carbons. Type-II is just between I and III. As explained in this review, it is highly recommended to synthesize Type-I or Type-II rather than Type-III; otherwise it is not possible to enjoy the specific and unique properties of ZTC.

In ZTC, it is possible to draw molecular models more accurately than the cases of other disordered nanoporous carbons, and this is beneficial to understand the fundamental relation between the molecular structure and properties/performance of nanoporous carbons. From their well-ordered and uniform graphene-based frameworks as well as the presence of a large amount of active edge sites, ZTCs have a good compatibility with chemical modifications, and therefore, their function can be further extended by either heteroatom doping or forming composites with other components.

ZTCs possess a high surface area up to ca. $4000 \text{ m}^2 \text{ g}^{-1}$, comparable to highly porous MOFs. Thus, ZTCs are competitive materials against MOFs regarding to the applications for adsorbents and gas storage applications. Though the microporosity is not as high as the best MOFs, ZTCs have great advantages of thermal stability, chemical stability, hydrophobicity, and a high thermal conductivity, as carbonaceous materials. ZTCs are useful also as stable catalysts supports, and moreover, their frameworks exhibit unique catalysis for some specific reactions. Unlike MOFs or organic-based nanoporous materials, ZTCs are electrically conductive, and can be used for electrode applications for electrochemical capacitors, rechargeable batteries, and fuel cells. For the electrochemical applications, to grasp the stable potential range is crucial, because it is often different from those of other nanoporous carbons due to the large amount of active edge sites in ZTCs.

We hope that this article well illustrates the major features and advantages of ZTCs, thereby providing the further understanding of science of nanoporous carbons and graphene-based frameworks.

Conflicts of interest

There are no conflicts to declare.

Acknowledgements

We acknowledge the financial support by JSPS KAKENHI Grant Number 15KK0196, 17H01042, 15H01999 and 15H03591, and also by JST Sakigake network. The authors acknowledge Dr M. Ouzzine and Mr K. Nomura for their support of summarizing the data related to this article.

Notes and references

- 1 T. Kyotani, *Bull. Chem. Soc. Jpn.*, 2006, **79**, 1322-1337.
- 2 K. Takai, T. Suzuki, T. Enoki, H. Nishihara and T. Kyotani, *Phys. Rev. B*, 2010, **81**, 205420.
- 3 T. Koretsune, R. Arita and H. Aoki, *Phys. Rev. B*, 2012, **86**, 125207.
- 4 T. Kyotani, T. Nagai, S. Inoue and A. Tomita, *Chem. Mater.*, 1997, **9**, 609-615.
- 5 H. Nishihara and T. Kyotani, in *Novel Carbon Adsorbents*, ed. J. M. D. Tascon, Elsevier, 2012, pp. 295-322.
- 6 A. L. Mackay and H. Terrones, *Nature*, 1991, **352**, 762.
- 7 T. Lenosky, X. Gonze, M. Teter and V. Elser, *Nature*, 1992, **355**, 333-335.
- 8 H. Nishihara, Q. H. Yang, P. X. Hou, M. Unno, S. Yamauchi, R. Saito, et al., *Carbon*, 2009, **47**, 1220-1230.
- 9 Z. X. Ma, T. Kyotani and A. Tomita, *Chem. Commun.*, 2000, 2365-2366.
- 10 Z. X. Ma, T. Kyotani, Z. Liu, O. Terasaki and A. Tomita, *Chem. Mater.*, 2001, **13**, 4413-4415.
- 11 H. Nishihara, H. Fujimoto, H. Itoi, K. Nomura, H. Tanaka, M. T. Miyahara, et al., *Carbon*, 2018, **129**, 854-862.
- 12 Z. X. Yang, Y. D. Xia, X. Z. Sun and R. Mokaya, *J. Phys. Chem. B*, 2006, **110**, 18424-18431.
- 13 M. Armandi, B. Bonelli, I. Bottero, C. O. Arean and E. Garrone, *Microporous Mesoporous Mater.*, 2007, **103**, 150-157.
- 14 L. Chen, R. K. Singh and P. Webley, *Microporous Mesoporous Mater.*, 2007, **102**, 159-170.
- 15 S. Lei, J. Miyamoto, T. Ohba, H. Kanoh and K. Kaneko, *J. Phys. Chem. C*, 2007, **111**, 2459-2464.
- 16 Z. X. Yang, Y. D. Xia and R. Mokaya, *J. Am. Chem. Soc.*, 2007, **129**, 1673-1679.
- 17 A. J. Lachawiec and R. T. Yang, *Langmuir*, 2008, **24**, 6159-6165.
- 18 A. Pacula and R. Mokaya, *J. Phys. Chem. C*, 2008, **112**, 2764-2769.
- 19 L. F. Wang and R. T. Yang, *J. Phys. Chem. C*, 2008, **112**, 12486-12494.
- 20 Y. X. Yang, R. K. Singh and P. A. Webley, *Adsorption*, 2008, **14**, 265-274.
- 21 C. Guan, K. Wang, C. Yang and X. S. Zhao, *Microporous Mesoporous Mater.*, 2009, **118**, 503-507.
- 22 C. Guan, X. Zhang, K. Wang and C. Yang, *Sep. Purif. Technol.*, 2009, **66**, 565-569.
- 23 H. Nishihara, P. X. Hou, L. X. Li, M. Ito, M. Uchiyama, T. Kaburagi, et al., *J. Phys. Chem. C*, 2009, **113**, 3189-3196.

- 24 R. Thomas, B. Christophe, E. G. Keith and J. M. P. Roland, *J. Chem. Phys.*, 2009, **130**, 174717.
- 25 H. L. Wang, Q. M. Gao, J. Hu and Z. Chen, *Carbon*, 2009, **47**, 2259-2268.
- 26 L. Wang, F. H. Yang and R. T. Yang, *AIChE J.*, 2009, **55**, 1823-1833.
- 27 Y. D. Xia, G. S. Walker, D. M. Grant and R. Mokaya, *J. Am. Chem. Soc.*, 2009, **131**, 16493-16499.
- 28 Y. X. Yang, L. Bourgeois, C. X. Zhao, D. Y. Zhao, A. Chaffee and P. A. Webley, *Microporous Mesoporous Mater.*, 2009, **119**, 39-46.
- 29 N. Alam and R. Mokaya, *Energy Environ. Sci.*, 2010, **3**, 1773-1781.
- 30 M. Kayanuma, U. Nagashima, H. Nishihara, T. Kyotani and H. Ogawa, *Chem. Phys. Lett.*, 2010, **495**, 251-255.
- 31 M. Sevilla, N. Alam and R. Mokaya, *J. Phys. Chem. C*, 2010, **114**, 11314-11319.
- 32 L. F. Wang and R. T. Yang, *Cat. Rev. -Sci. Eng.*, 2010, **52**, 411-461.
- 33 Z. Wang, F. H. Yang and R. T. Yang, *J. Phys. Chem. C*, 2010, **114**, 1601-1609.
- 34 Y. Xia, Z. Yang and R. Mokaya, *Chem. Vap. Deposition*, 2010, **16**, 322-328.
- 35 N. Alam and R. Mokaya, *Microporous Mesoporous Mater.*, 2011, **142**, 716-724.
- 36 N. Alam and R. Mokaya, *Microporous Mesoporous Mater.*, 2011, **144**, 140-147.
- 37 M. Armandi, B. Bonelli, K. Cho, R. Ryoo and E. Garrone, *Int. J. Hydrogen Energy*, 2011, **36**, 7937-7943.
- 38 C. M. Ghimbeu, C. Zlotea, R. Gadiou, F. Cuevas, E. Leroy, M. Latroche, et al., *J. Mater. Chem.*, 2011, **21**, 17765-17775.
- 39 K. Suzuki, M. Kayanuma, M. Tachikawa, H. Ogawa, H. Nishihara, T. Kyotani, et al., *Compt. Theoret. Chem.*, 2011, **975**, 128-133.
- 40 K. Suzuki, M. Kayanuma, M. Tachikawa, H. Ogawa, H. Nishihara, T. Kyotani, et al., *J. Alloys Compd.*, 2011, **509**, S868-S871.
- 41 K. Suzuki, M. Tachikawa, H. Ogawa, S. Ittisanronnachai, H. Nishihara, T. Kyotani, et al., *Theor. Chem. Acc.*, 2011, **130**, 1039-1042.
- 42 Y. Xia, R. Mokaya, D. M. Grant and G. S. Walker, *Carbon*, 2011, **49**, 844-853.
- 43 Y. Yang, C. M. Brown, C. Zhao, A. L. Chaffee, B. Nick, D. Zhao, et al., *Carbon*, 2011, **49**, 1305-1317.
- 44 S. Y. Lee and S. J. Park, *J. Colloid Interface Sci.*, 2012, **384**, 116-120.
- 45 E. Masika and R. Mokaya, *J. Phys. Chem. C*, 2012, **116**, 25734-25740.
- 46 N. P. Stadie, J. J. Vajo, R. W. Cumberland, A. A. Wilson, C. C. Ahn and B. Fultz, *Langmuir*, 2012, **28**, 10057-10063.
- 47 T. G. Voskuilen, T. L. Pourpoint and A. M. Dailly, *Adsorption*, 2012, **18**, 239-249.
- 48 L. Wang and R. T. Yang, *Carbon*, 2012, **50**, 3134-3140.
- 49 S. J. Yang, J. H. Im, H. Nishihara, H. Jung, K. Lee, T. Kyotani, et al., *J. Phys. Chem. C*, 2012, **116**, 10529-10540.
- 50 R. J. Konwar and M. De, *Microporous Mesoporous Mater.*, 2013, **175**, 16-24.
- 51 E. Masika, R. A. Bourne, T. W. Chamberlain and R. Mokaya, *ACS Appl. Mater. Interfaces*, 2013, **5**, 5639-5647.
- 52 E. Masika and R. Mokaya, *Prog. Nat. Sci.*, 2013, **23**, 308-316.
- 53 Y. Xia, Z. Yang, X. Gou and Y. Zhu, *Int. J. Hydrogen Energy*, 2013, **38**, 5039-5052.
- 54 J. Cai, L. Li, X. Lv, C. Yang and X. Zhao, *ACS Appl. Mater. Interfaces*, 2014, **6**, 167-175.
- 55 J. Cai, M. Yang, Y. Xing and X. Zhao, *Colloids Surf. A*, 2014, **444**, 240-245.
- 56 E. Masika and R. Mokaya, *Energy Environ. Sci.*, 2014, **7**, 427-434.
- 57 H. Nishihara, S. Ittisanronnachai, H. Itoi, L. X. Li, K. Suzuki, U. Nagashima, et al., *J. Phys. Chem. C*, 2014, **118**, 9551-9559.
- 58 Z. Geng, C. Zhang, D. Wang, X. Zhou and M. Cai, *J. Energy Chem.*, 2015, **24**, 1-8.
- 59 R. J. Konwar and M. De, *Int. J. Energy Res.*, 2015, **39**, 223-233.
- 60 N. M. Musyoka, J. Ren, H. W. Langmi, B. C. North and M. Mathe, *Int. J. Hydrogen Energy*, 2015, **40**, 12705-12712.
- 61 N. M. Musyoka, J. Ren, H. W. Langmi, D. E. C. Rogers, B. C. North, M. Mathe, et al., *Int. J. Energy Res.*, 2015, **39**, 494-503.
- 62 J. Shao, X. Xiao, X. Fan, X. Huang, B. Zhai, S. Li, et al., *Nano Energy*, 2015, **15**, 244-255.
- 63 C. Yong Liang Guana, A. Elkamel and K. Wang, *Can. J. Chem. Eng.*, 2015, **93**, 527-531.
- 64 N. Balahmar, A. M. Lowbridge and R. Mokaya, *J. Mater. Chem. A*, 2016, **4**, 14254-14266.
- 65 R. J. Konwar and M. De, *Int. J. Hydrogen Energy*, 2016, **41**, 21300-21309.
- 66 N. M. Musyoka, J. Ren, P. Annamalai, H. W. Langmi, B. C. North, M. Mathe, et al., *Res. Chem. Intermed.*, 2016, **42**, 5299-5307.
- 67 Z. Yang, W. Xiong, J. Wang, Y. Zhu and Y. Xia, *Eur. J. Inorg. Chem.*, 2016, **2016**, 2152-2158.
- 68 P. Annamalai, N. M. Musyoka, J. Ren, H. W. Langmi, M. Mathe, D. Bessarabov, et al., *Res. Chem. Intermed.*, 2017, **43**, 4095-4102.
- 69 H. Itoi, H. Nishihara, S. Kobayashi, S. Ittisanronnachai, T. Ishii, R. Berenguer, et al., *J. Phys. Chem. C*, 2017, **121**, 7892-7902.
- 70 A. Martínez de Yuso, M. De Fina, C. Nita, P. Fioux, J. Parmentier and C. Matei Ghimbeu, *Microporous Mesoporous Mater.*, 2017, **243**, 135-146.
- 71 C. O. Ania, V. Khomenko, E. Raymundo-Pinero, J. B. Parra and F. Beguin, *Adv. Funct. Mater.*, 2007, **17**, 1828-1836.
- 72 H. Nishihara, H. Itoi, T. Kogure, P. X. Hou, H. Touhara, F. Okino, et al., *Chem.-Eur. J.*, 2009, **15**, 5355-5363.
- 73 C. Portet, Z. Yang, Y. Korenblit, Y. Gogotsi, R. Mokaya and G. Yushin, *J. Electrochem. Soc.*, 2009, **156**, A1-A6.
- 74 A. Kajdos, A. Kvit, F. Jones, J. Jagiello and G. Yushin, *J. Am. Chem. Soc.*, 2010, **132**, 3252-3253.
- 75 H. Wang, Q. Gao and J. Hu, *Microporous Mesoporous Mater.*, 2010, **131**, 89-96.
- 76 H. Xu, Q. Gao, H. Guo and H. Wang, *Microporous Mesoporous Mater.*, 2010, **133**, 106-114.
- 77 H. Itoi, H. Nishihara, T. Kogure and T. Kyotani, *J. Am. Chem. Soc.*, 2011, **133**, 1165-1167.
- 78 W. Li, J. Zhou, W. Xing, S. P. Zhuo and Y. M. Lu, *Acta Phys. Chim. Sin.*, 2011, **27**, 620-626.

- 79 X. Wu, X. Hong, J. Nan, Z. Luo, Q. Zhang, L. Li, et al., *Microporous Mesoporous Mater.*, 2012, **160**, 25-31.
- 80 A. Berenguer-Murcia, R. R. Ruiz-Rosas, J. Garcia-Aguilar, K. Nueangnoraj, H. Nishihara, E. Morallon, et al., *Phys. Chem. Chem. Phys.*, 2013, **15**, 10331-10334.
- 81 K. Kim, M. Choi and R. Ryoo, *Carbon*, 2013, **60**, 175-185.
- 82 K. Nueangnoraj, H. Nishihara, K. Imai, H. Itoi, T. Ishii, M. Kiguchi, et al., *Carbon*, 2013, **62**, 455-464.
- 83 Y. Wang, H. Sun, R. Zhang, S. Yu and J. Kong, *Carbon*, 2013, **53**, 245-251.
- 84 H. Itoi, H. Nishihara, T. Ishii, K. Nueangnoraj, R. Berenguer-Betrian and T. Kyotani, *Bull. Chem. Soc. Jpn.*, 2014, **87**, 250-257.
- 85 H. Luo, F. Zhang, X. Zhao, Y. Sun, K. Du and H. Feng, *J. Mater. Sci.-Mater. Electron.*, 2014, **25**, 538-545.
- 86 K. Nueangnoraj, R. Ruiz-Rosas, H. Nishihara, S. Shiraishi, E. Morallon, D. Cazorla-Amoros, et al., *Carbon*, 2014, **67**, 792-794.
- 87 R. Ruiz-Rosas, M. J. Valero-Romero, D. Salinas-Torres, J. Rodríguez-Mirasol, T. Cordero, E. Morallón, et al., *ChemSusChem*, 2014, **7**, 1458-1467.
- 88 J. S. Moon, H. Kim, D. C. Lee, J. T. Lee and G. Yushin, *J. Electrochem. Soc.*, 2015, **162**, A5070-A5076.
- 89 K. Nueangnoraj, H. Nishihara, T. Ishii, N. Yamamoto, H. Itoi, R. Berenguer, et al., *Energy Storage Mater.*, 2015, **1**, 35-41.
- 90 C. González-Gaitán, R. Ruiz-Rosas, H. Nishihara, T. Kyotani, E. Morallón and D. Cazorla-Amorós, *Carbon*, 2016, **99**, 157-166.
- 91 H. Itoi, H. Nishihara and T. Kyotani, *Langmuir*, 2016, **32**, 11997-12004.
- 92 J. M. Rosas, R. Ruiz-Rosas, R. Berenguer, D. Cazorla-Amoros, E. Morallon, H. Nishihara, et al., *J. Mater. Chem. A*, 2016, **4**, 4610-4618.
- 93 M. Stojmenović, M. Vujković, L. Matović, J. Krstić, A. Đukić, V. Dodevski, et al., *Microporous Mesoporous Mater.*, 2016, **228**, 94-106.
- 94 A. Castro-Muniz, H. Nishihara, T. Hirota, M. Ohwada, L. X. Li, T. Tsuda, et al., *Chem. Commun.*, 2017, **53**, 13348-13351.
- 95 M. J. Mostazo-López, R. Ruiz-Rosas, A. Castro-Muñoz, H. Nishihara, T. Kyotani, E. Morallón, et al., *Carbon*, 2018, **129**, 510-519.
- 96 M. T. Gilbert, J. H. Knox and B. Kaur, *Chromatographia*, 1982, **16**, 138-148.
- 97 R. W. Pekala and R. W. Hopper, *J. Membr. Sci.*, 1987, **22**, 1840-1844.
- 98 T. Kyotani, N. Sonobe and A. Tomita, *Nature*, 1988, **331**, 331-333.
- 99 T. Kyotani, L. F. Tsai and A. Tomita, *Chem. Mater.*, 1995, **7**, 1427-1428.
- 100 T. Kyotani, L. F. Tsai and A. Tomita, *Chem. Mater.*, 1996, **8**, 2109-2113.
- 101 G. Che, B. B. Lakshmi, C. R. Martin, E. R. Fisher and R. S. Ruoff, *Chem. Mater.*, 1998, **10**, 260-267.
- 102 G. L. Che, B. B. Lakshmi, E. R. Fisher and C. R. Martin, *Nature*, 1998, **393**, 346-349.
- 103 S. A. Johnson, E. S. Brigham, P. J. Ollivier and T. E. Mallouk, *Chem. Mater.*, 1997, **9**, 2448-2458.
- 104 J. Rodriguez-Mirasol, T. Cordero, L. R. Radovic and J. J. Rodriguez, *Chem. Mater.*, 1998, **10**, 550-558.
- 105 A. A. Zakhidov, R. H. Baughman, Z. Iqbal, C. X. Cui, I. Khayrullin, S. O. Dantas, et al., *Science*, 1998, **282**, 897-901.
- 106 R. Ryoo, S. H. Joo and S. Jun, *J. Phys. Chem. B*, 1999, **103**, 7743-7746.
- 107 J. Lee, S. Yoon, T. Hyeon, S. M. Oh and K. B. Kim, *Chem. Commun.*, 1999, 2177-2178.
- 108 C. D. Liang, K. L. Hong, G. A. Guiochon, J. W. Mays and S. Dai, *Angew. Chem. Int. Ed.*, 2004, **43**, 5785-5789.
- 109 S. Tanaka, N. Nishiyama, Y. Egashira and K. Ueyama, *Chem. Commun.*, 2005, 2125-2127.
- 110 Y. Meng, D. Gu, F. Q. Zhang, Y. F. Shi, H. F. Yang, Z. Li, et al., *Angew. Chem. Int. Ed.*, 2005, **44**, 7053-7059.
- 111 B. Liu, H. Shioyama, T. Akita and Q. Xu, *J. Am. Chem. Soc.*, 2008, **130**, 5390-5391.
- 112 H. L. Jiang, B. Liu, Y. Q. Lan, K. Kuratani, T. Akita, H. Shioyama, et al., *J. Am. Chem. Soc.*, 2011, **133**, 11854-11857.
- 113 L. Radhakrishnan, J. Reboul, S. Furukawa, P. Srinivasu, S. Kitagawa and Y. Yamauchi, *Chem. Mater.*, 2011, **23**, 1225-1231.
- 114 M. Hu, J. Reboul, S. Furukawa, L. Radhakrishnan, Y. Zhang, P. Srinivasu, et al., *Chem. Commun.*, 2011, **47**, 8124-8126.
- 115 W. Chaikittisilp, M. Hu, H. Wang, H. S. Huang, T. Fujita, K. C. Wu, et al., *Chem. Commun.*, 2012, **48**, 7259-7261.
- 116 M. Hu, J. Reboul, S. Furukawa, N. L. Torad, Q. Ji, P. Srinivasu, et al., *J. Am. Chem. Soc.*, 2012, **134**, 2864-2867.
- 117 S. Lim, K. Suh, Y. Kim, M. Yoon, H. Park, D. N. Dybtsev, et al., *Chem. Commun.*, 2012, **48**, 7447-7449.
- 118 S. J. Yang, T. Kim, J. H. Im, Y. S. Kim, K. Lee, H. Jung, et al., *Chem. Mater.*, 2012, **24**, 464-470.
- 119 H. B. Aiyappa, P. Pachfule, R. Banerjee and S. Kurungot, *Cryst. Growth Des.*, 2013, **13**, 4195-4199.
- 120 W. Chaikittisilp, K. Ariga and Y. Yamauchi, *J. Mater. Chem. A*, 2013, **1**, 14.
- 121 E. Kayahara, T. Iwamoto, H. Takaya, T. Suzuki, M. Fujitsuka, T. Majima, et al., *Nat. Commun.*, 2013, **4**, 2694.
- 122 N. L. Torad, M. Hu, Y. Kamachi, K. Takai, M. Imura, M. Naito, et al., *Chem. Commun.*, 2013, **49**, 2521-2523.
- 123 S. J. Yang, S. Nam, T. Kim, J. H. Im, H. Jung, J. H. Kang, et al., *J. Am. Chem. Soc.*, 2013, **135**, 7394-7397.
- 124 H. B. Wu and X. W. Lou, *Sci. Adv.*, 2017, **3**,
- 125 H. Nishihara, T. Hirota, K. Matsuura, M. Ohwada, N. Hoshino, T. Akutagawa, et al., *Nat. Commun.*, 2017, **8**, 109.
- 126 Z. P. Chen, W. C. Ren, L. B. Gao, B. L. Liu, S. F. Pei and H. M. Cheng, *Nat. Mater.*, 2011, **10**, 424-428.
- 127 H. Nishihara, T. Shimura, S. Kobayashi, K. Nomura, R. Berenguer, M. Ito, et al., *Adv. Funct. Mater.*, 2016, **26**, 6418-6427.
- 128 C. J. Meyers, S. D. Shah, S. C. Patel, R. M. Sneeringer, C. A. Bessel, N. R. Dollahon, et al., *J. Phys. Chem. B*, 2001, **105**, 2143-2152.
- 129 P. M. Barata-Rodrigues, T. J. Mays and G. D. Moggridge, *Carbon*, 2003, **41**, 2231-2246.
- 130 T. Kyotani, Z. X. Ma and A. Tomita, *Carbon*, 2003, **41**, 1451-1459.

- 131 L. Tosheva, J. Parmentier, V. Valtchev, C. Vix-Guterl and J. Patarin, *Carbon*, 2005, **43**, 2474-2480.
- 132 Z. X. Yang, Y. D. Xia and R. Mokaya, *Microporous Mesoporous Mater.*, 2005, **86**, 69-80.
- 133 J. Parmentier, V. Valtchev, F. Gaslain, L. Tosheva, C. Ducrot-Boisgontier, J. Möller, et al., *Carbon*, 2009, **47**, 1066-1073.
- 134 M. J. Valero-Romero, E. M. Márquez-Franco, J. Bedia, J. Rodríguez-Mirasol and T. Cordero, *Microporous Mesoporous Mater.*, 2014, **196**, 68-78.
- 135 K. Kim, T. Lee, Y. Kwon, Y. Seo, J. Song, J. K. Park, et al., *Nature*, 2016, **535**, 131-135.
- 136 Y. Kwon, K. Kim and R. Ryoo, *RSC Adv.*, 2016, **6**, 43091-43097.
- 137 J. Wang, Z. Liu, X. Dong, C. E. Hsiung, Y. Zhu, L. Liu, et al., *J. Mater. Chem. A*, 2017, **5**, 6860-6865.
- 138 F. O. M. Gaslain, J. Parmentier, V. P. Valtchev and J. Patarin, *Chem. Commun.*, 2006, 991-993.
- 139 C. Ducrot-Boisgontier, J. Parmentier, L. Delmotte and J. Patarin, *J. Membr. Sci.*, 2009, **44**, 6571.
- 140 C. Ducrot-Boisgontier, J. Parmentier and J. Patarin, *Microporous Mesoporous Mater.*, 2009, **126**, 101-106.
- 141 S. Builes, T. Roussel, C. M. Ghimbeu, J. Parmentier, R. Gadiou, C. Vix-Guterl, et al., *Phys. Chem. Chem. Phys.*, 2011, **13**, 16063-16070.
- 142 Y. Xia, R. Mokaya, G. S. Walker and Y. Zhu, *Adv. Energy Mater.*, 2011, **1**, 678-683.
- 143 Y. Xia, Y. Zhu and Y. Tang, *Carbon*, 2012, **50**, 5543-5553.
- 144 J. Parmentier, F. O. Gaslain, O. Ersen, T. A. Centeno and L. A. Solovyov, *Langmuir*, 2014, **30**, 297-307.
- 145 L. Wang and R. T. Yang, *J. Phys. Chem. C*, 2012, **116**, 1099-1106.
- 146 Z. X. Ma, T. Kyotani and A. Tomita, *Carbon*, 2002, **40**, 2367-2374.
- 147 F. Su, X. S. Zhao, L. Lv and Z. Zhou, *Carbon*, 2004, **42**, 2821-2831.
- 148 A. Garsuch and O. Klepel, *Carbon*, 2005, **43**, 2330-2337.
- 149 P. X. Hou, H. Orikasa, T. Yamazaki, K. Matsuoka, A. Tomita, N. Setoyama, et al., *Chem. Mater.*, 2005, **17**, 5187-5193.
- 150 P. X. Hou, T. Yamazaki, H. Orikasa and T. Kyotani, *Carbon*, 2005, **43**, 2624-2627.
- 151 K. Matsuoka, Y. Yamagishi, T. Yamazaki, N. Setoyama, A. Tomita and T. Kyotani, *Carbon*, 2005, **43**, 876-879.
- 152 J. I. Paredes, A. Martínez-Alonso, T. Yamazaki, K. Matsuoka, J. M. D. Tascon and T. Kyotani, *Langmuir*, 2005, **21**, 8817-8823.
- 153 F. Su, L. Lv, T. M. Hui and X. S. Zhao, *Carbon*, 2005, **43**, 1156-1164.
- 154 F. B. Su, H. J. Zeng, Y. J. Yu, L. Lv, J. Y. Lee and X. S. Zhao, *Carbon*, 2005, **43**, 2366-2373.
- 155 A. Garsuch, O. Klepel, R. R. Sattler, C. Berger, R. Gläser and J. Weitkamp, *Carbon*, 2006, **44**, 593-596.
- 156 A. Garsuch, R. R. Sattler, S. Witt and O. Klepel, *Microporous Mesoporous Mater.*, 2006, **89**, 164-169.
- 157 J. I. Paredes, A. Martínez-Alonso, P. X. Hou, T. Kyotani and J. M. D. Tascón, *Carbon*, 2006, **44**, 2469-2478.
- 158 T. Roussel, J. Jagiello, R. J. M. Pellenq, M. Thommes and C. Bichara, *Molecular Simulation*, 2006, **32**, 551-555.
- 159 P. X. Hou, H. Orikasa, H. Itoi, H. Nishihara and T. Kyotani, *Carbon*, 2007, **45**, 2011-2016.
- 160 O. Klepel, H. Strauß, A. Garsuch and K. Böhme, *Mater. Lett.*, 2007, **61**, 2037-2039.
- 161 T. Roussel, A. Didion, R. J. M. Pellenq, R. Gadiou, C. Bichara and C. Vix-Guterl, *J. Phys. Chem. C*, 2007, **111**, 15863-15876.
- 162 X. Yuan, S. P. Zhuo, W. Xing, H. Y. Cui, X. D. Dai, X. M. Liu, et al., *J. Colloid Interface Sci.*, 2007, **310**, 83-89.
- 163 C. Guan, F. Su, X. S. Zhao and K. Wang, *Sep. Purif. Technol.*, 2008, **64**, 124-126.
- 164 R. M. Freire, A. H. de Moraes Batista, A. G. de Souza Filho, J. M. Filho, G. D. Saraiva and A. C. Oliveira, *Catal. Lett.*, 2009, **131**, 135-145.
- 165 L. Ji, F. Liu, Z. Xu, S. Zheng and D. Zhu, *Environ. Sci. Technol.*, 2009, **43**, 7870-7876.
- 166 C. Ducrot-Boisgontier, J. Parmentier, A. Faour, J. Patarin and G. D. Pirngruber, *Energy Fuels*, 2010, **24**, 3595-3602.
- 167 L. Ji, F. Liu, Z. Xu, S. Zheng and D. Zhu, *Environ. Sci. Technol.*, 2010, **44**, 3116-3122.
- 168 Y. Kinoshita, R. Toda, T. Matsushita, M. Hieda, N. Wada, H. Nishihara, et al., *J. Low Temp. Phys.*, 2010, **158**, 275-280.
- 169 A. M. Puziy, O. I. Poddubnaya, B. Gawdzik, M. Sobiesiak, C. A. Reinish, M. M. Tsyba, et al., *Appl. Surf. Sci.*, 2010, **256**, 5216-5220.
- 170 K. Takai, T. Suzuki, T. Enoki, H. Nishihara and T. Kyotani, *J. Phys. Chem. Solids*, 2010, **71**, 565-568.
- 171 C. Guan, L. S. Loo, K. Wang and C. Yang, *Energy Conversion and Management*, 2011, **52**, 1258-1262.
- 172 Y. Nakashima, T. Matsushita, M. Hieda, N. Wada, H. Nishihara and T. Kyotani, *J. Low Temp. Phys.*, 2011, **162**, 565-572.
- 173 H. K. Youn, J. Kim, G. Chandrasekar, H. Jin and W. S. Ahn, *Mater. Lett.*, 2011, **65**, 1772-1774.
- 174 A. Y. Lo, C. T. Hung, N. Yu, C. T. Kuo and S. B. Liu, *Appl. Energy*, 2012, **100**, 66-74.
- 175 X. H. Song, W. S. Teo and K. Wang, *J. Porous Mater.*, 2012, **19**, 211-215.
- 176 K. Takai, T. Suzuki, H. Nishihara, T. Kyotani and T. Enoki, *J. Phys. Chem. Solids*, 2012, **73**, 1436-1439.
- 177 H. N. Yang, J. Y. Lee, Y. Na, S. C. Yi and W. J. Kim, *Microporous Mesoporous Mater.*, 2012, **152**, 148-156.
- 178 Y. Yang, L. Tang, N. Burke and K. Chiang, *J. Nanopart. Res.*, 2012, **14**, 1028.
- 179 B. Zhang, Y. Wu, F. Meng, T. Xu, J. Zhu and M. Sun, *Procedia Eng.*, 2012, **27**, 762-767.
- 180 J. Zhou, W. Li, Z. Zhang, W. Xing and S. Zhuo, *RSC Adv.*, 2012, **2**, 161-167.
- 181 R. Berenguer, H. Nishihara, H. Itoi, T. Ishii, E. Morallon, D. Cazorla-Amoros, et al., *Carbon*, 2013, **54**, 94-104.
- 182 K. Fukuhara, K. Nakajima, M. Kitano, S. Hayashi and M. Hara, *Phys. Chem. Chem. Phys.*, 2013, **15**, 9343-9350.
- 183 M. Ito, H. Nishihara, K. Yamamoto, H. Itoi, H. Tanaka, A. Maki, et al., *Chem.-Eur. J.*, 2013, **19**, 13009-13016.
- 184 H. Kyakuno, K. Matsuda, Y. Nakai, T. Fukuoka, Y. Maniwa, H. Nishihara, et al., *Chem. Phys. Lett.*, 2013, **571**, 54-60.
- 185 Y. Lv, Z. Wu, X. Qian, Y. Fang, D. Feng, Y. Xia, et al., *ChemSusChem*, 2013, **6**, 1938-1944.

- 186 X. H. Song, R. Xu and K. Wang, *J. Anal. Appl. Pyrolysis*, 2013, **100**, 153-157.
- 187 N. P. Stadie, M. Murialdo, C. C. Ahn and B. Fultz, *J. Am. Chem. Soc.*, 2013, **135**, 990-993.
- 188 H. N. Yang, S. H. Park, D. C. Lee, S. C. Yi and W. J. Kim, *Microporous Mesoporous Mater.*, 2013, **172**, 161-166.
- 189 W. Donphai, T. Kamegawa, M. Chareonpanich, K. Nueangnoraj, H. Nishihara, T. Kyotani, et al., *Phys. Chem. Chem. Phys.*, 2014, **16**, 25004-25007.
- 190 M. Enterría, F. Suárez-García, A. Martínez-Alonso and J. M. D. Tascón, *Microporous Mesoporous Mater.*, 2014, **190**, 156-164.
- 191 C. X. Jiang, K. Hara, K. Namba, H. Kobayashi, S. Ittisanronnachai, H. Nishihara, et al., *Chem. Lett.*, 2014, **43**, 1794-1796.
- 192 T. J. Lim, S. Y. Lee, Y. J. Yoo and S. J. Park, *Bull. Korean Chem. Soc.*, 2014, **35**, 3576-3582.
- 193 L. Yingying, W. Zhangxiong, F. Yin, Q. Xufang, M. A. Abdullah, T. Bo, et al., *APL Mater.*, 2014, **2**, 113302.
- 194 P. W. Chung, M. Yabushita, A. T. To, Y. Bae, J. Jankolovits, H. Kobayashi, et al., *ACS Catal.*, 2015, **5**, 6422-6425.
- 195 C. Matei Ghimbeu, K. Guerin, M. Dubois, S. Hajjar-Garreau and C. Vix-Guterl, *Carbon*, 2015, **84**, 567-583.
- 196 M. Murialdo, N. P. Stadie, C. C. Ahn and B. Fultz, *J. Phys. Chem. C*, 2015, **119**, 944-950.
- 197 M. Murialdo, N. P. Stadie, C. C. Ahn and B. Fultz, *Langmuir*, 2015, **31**, 7991-7998.
- 198 J. Shi, W. Li and D. Li, *Colloids Surf. A*, 2015, **485**, 11-17.
- 199 N. P. Stadie, M. Murialdo, C. C. Ahn and B. Fultz, *J. Phys. Chem. C*, 2015, **119**, 26409-26421.
- 200 H. Goto, T. Tajima, K. Kobayashi, Y. Takaguchi, K. Nueangnoraj and H. Nishihara, *Chem. Lett.*, 2016, **45**, 601-603.
- 201 O. Klepel, N. Danneberg, M. Dräger, M. Erlitz and M. Taubert, *Materials*, 2016, **9**, 214.
- 202 M. Murialdo, N. P. Stadie, C. C. Ahn and B. Fultz, *J. Phys. Chem. C*, 2016, **120**, 11847-11853.
- 203 K. Nueangnoraj, T. Tomai, H. Nishihara, T. Kyotani and I. Honma, *Carbon*, 2016, **107**, 831-836.
- 204 A. M. Panich, V. Y. Osipov, H. Nishihara and T. Kyotani, *Synth. Met.*, 2016, **221**, 149-152.
- 205 M. Yabushita, K. Techikawara, H. Kobayashi, A. Fukuoka and A. Katz, *ACS Sustain. Chem. Eng.*, 2016, **4**, 6844-6851.
- 206 C. J. Elles-Pérez, A. Muñoz-Acevedo, A. Guzmán, H. Camargo and J. Henao, *J. Environ. Manage.*, 2017, **196**, 466-475.
- 207 N. P. Stadie, S. Wang, K. V. Kravchuk and M. V. Kovalenko, *ACS Nano*, 2017, **11**, 1911-1919.
- 208 E. N. Coker, W. A. Steen and J. E. Miller, *Microporous Mesoporous Mater.*, 2007, **104**, 236-247.
- 209 E. N. Coker, W. A. Steen, J. T. Miller, A. J. Kropf and J. E. Miller, *Microporous Mesoporous Mater.*, 2007, **101**, 440-444.
- 210 M. Seredych and T. J. Bandoz, *Microporous Mesoporous Mater.*, 2007, **100**, 45-54.
- 211 M. Seredych and T. J. Bandoz, *Langmuir*, 2007, **23**, 6033-6041.
- 212 C. Wang, C. Yan, J. Yao, L. Zhang, N. Xu and X. Liu, *J. Porous Mater.*, 2008, **16**, 699.
- 213 C. Yan, C. Wang, J. Yao, L. Zhang and X. Liu, *Colloids Surf. A*, 2009, **333**, 115-119.
- 214 S. Choi, H. Kim, S. Lee, Y. Wang, C. Ercan, R. Othman, et al., *Chem. Eng. J.*, 2015, **280**, 597-605.
- 215 C. H. Choi, M. Kim, H. C. Kwon, S. J. Cho, S. Yun, H. T. Kim, et al., *Nat. Commun.*, 2016, **7**, 10922.
- 216 Y. Cui, J. Chen, K. Huang, C. Du, J. Wu, A. P. Baker, et al., *RSC Adv.*, 2016, **6**, 9117-9123.
- 217 K. Kim, Y. Kwon, T. Lee, S. J. Cho and R. Ryoo, *Carbon*, 2017, **118**, 517-523.
- 218 H. Nishihara, K. Imai, H. Itoji, K. Nomura, K. Takai and T. Kyotani, *Tanso*, 2017, **280**, 169-174.
- 219 L. Liu, D. Ma, H. Zheng, X. Li, M. Cheng and X. Bao, *Microporous Mesoporous Mater.*, 2008, **110**, 216-222.
- 220 V. K. Saini, M. L. Pinto and J. Pires, *Mater. Chem. Phys.*, 2013, **138**, 877-885.
- 221 P. Asgarian, A. Nourbakhsh, P. Amin, R. Ebrahimi-Kahrizsangi and K. J. D. MacKenzie, *Ceram. Int.*, 2014, **40**, 16399-16408.
- 222 C. Wang, R. Ma, Q. Wu, M. Sun and Z. Wang, *J. Chromatogr. A*, 2014, **1361**, 60-66.
- 223 L. Liu, Y. Hao, X. Zhou, C. Wang, Q. Wu and Z. Wang, *Anal. Methods*, 2015, **7**, 2762-2769.
- 224 B. S. Mojarad, A. Nourbakhsh, R. E. Kahrizsangi, M. Masoud and K. J. D. MacKenzie, *Ceram. Int.*, 2015, **41**, 5287-5293.
- 225 Q. Wu, X. Zhou, M. Sun, X. Ma, C. Wang and Z. Wang, *Microchim. Acta*, 2015, **182**, 879-885.
- 226 Y. Mu, N. Wang, Z. Sun, J. Wang, J. Li and J. Yu, *Chem. Sci.*, 2016, **7**, 3564-3568.
- 227 Y. Mu, H. Shi, Y. Wang, H. Ding and J. Li, *J. Mater. Chem. C*, 2017, **5**, 10894-10899.
- 228 B. Sakintuna and Y. Yürüm, *Microporous Mesoporous Mater.*, 2006, **93**, 304-312.
- 229 Y. Orooji, M. Kazemzad, Y. Ganjkanlou, A. A. Youzbashi and A. Khanlarkhani, *IET Micro Nano Lett.*, 2012, **7**, 1136-1139.
- 230 H. G. Baldovi, S. Valencia, M. Alvaro, A. M. Asiri and H. Garcia, *Nanoscale*, 2015, **7**, 1744-1752.
- 231 Y. Wang, Y. Li, Y. Yan, J. Xu, B. Guan, Q. Wang, et al., *Chem. Commun.*, 2013, **49**, 9006-9008.
- 232 C. Xue, H. Zhu, T. Xu, E. Wang, B. Xiao, X. Liu, et al., *RSC Adv.*, 2017, **7**, 24195-24203.
- 233 P. Srinivasu, A. Vinu, N. Gokulakrishnan, S. Anandan, A. Asthana, T. Mori, et al., *J. Nanosci. Nanotechnol.*, 2007, **7**, 2913-2916.
- 234 P. Srinivasu, A. Vinu, S. Hishita, T. Sasaki, K. Ariga and T. Mori, *Microporous Mesoporous Mater.*, 2008, **108**, 340-344.
- 235 D. Barrera, J. Villarroel-Rocha, J. C. Tara, E. I. Basaldella and K. Sapag, *Adsorption*, 2014, **20**, 967-976.
- 236 Z. K. Tang, H. D. Sun, J. Wang, J. Chen and G. Li, *Appl. Phys. Lett.*, 1998, **73**, 2287-2289.
- 237 L. Zuo, W. Song, T. Shi, C. Lv, J. Yao, J. Liu, et al., *Microporous Mesoporous Mater.*, 2014, **200**, 174-181.

- 238 Z. K. Tang, L. Y. Zhang, N. Wang, X. X. Zhang, G. H. Wen, G. D. Li, et al., *Science*, 2001, **292**, 2462-2465.
- 239 Y. Xiu, Q. Gao, G. D. Li, K. X. Wang and J. S. Chen, *Inorg. Chem.*, 2010, **49**, 5859-5867.
- 240 M. K. Antoniou, E. K. Diamanti, A. Enotiadis, A. Pollicchio, K. Dimos, F. Ciuchi, et al., *Microporous Mesoporous Mater.*, 2014, **188**, 16-22.
- 241 K. Hernadi, A. Fonseca, J. B. Nagy, D. Bemaerts, A. Fudala and A. A. Lucas, *Zeolites*, 1996, **17**, 416-423.
- 242 K. Mukhopadhyay, A. Koshio, T. Sugai, N. Tanaka, H. Shinohara, Z. Konya, et al., *Chem. Phys. Lett.*, 1999, **303**, 117-124.
- 243 D. N. Futaba, K. Hata, T. Yamada, T. Hiraoka, Y. Hayamizu, Y. Kakudate, et al., *Nat. Mater.*, 2006, **5**, 987-994.
- 244 M. D. Stoller, S. J. Park, Y. W. Zhu, J. H. An and R. S. Ruoff, *Nano Lett.*, 2008, **8**, 3498-3502.
- 245 K. Kaneko, C. Ishii, M. Ruike and H. Kuwabara, *Carbon*, 1992, **30**, 1075-1088.
- 246 Z. J. Fan, J. Yan, L. J. Zhi, Q. Zhang, T. Wei, J. Feng, et al., *Adv. Mater.*, 2010, **22**, 3723-3728.
- 247 Y. Wang, C. X. Guo, X. Wang, C. Guan, H. Yang, K. Wang, et al., *Energy Environ. Sci.*, 2011, **4**, 195-200.
- 248 S. Y. Yang, K. H. Chang, H. W. Tien, Y. F. Lee, S. M. Li, Y. S. Wang, et al., *J. Mater. Chem.*, 2011, **21**, 2374-2380.
- 249 K. W. Chen, L. B. Chen, Y. Q. Chen, H. Bai and L. Li, *J. Mater. Chem.*, 2012, **22**, 20968-20976.
- 250 L. Chen, X. Wang, X. Zhang and H. Zhang, *J. Mater. Chem.*, 2012, **22**, 22090.
- 251 F. Liu, S. Chung, G. Oh and T. S. Seo, *ACS Appl. Mater. Interfaces*, 2012, **4**, 922-927.
- 252 Z. S. Wu, Y. Sun, Y. Z. Tan, S. B. Yang, X. L. Feng and K. Mullen, *J. Am. Chem. Soc.*, 2012, **134**, 19532-19535.
- 253 Y. Ito, Y. Tanabe, H. J. Qiu, K. Sugawara, S. Heguri, N. H. Tu, et al., *Angew. Chem. Int. Ed.*, 2014, **53**, 4822-4826.
- 254 C. Lee, X. D. Wei, J. W. Kysar and J. Hone, *Science*, 2008, **321**, 385-388.
- 255 Y. He, W. Zhou, G. Qian and B. Chen, *Chem. Soc. Rev.*, 2014, **43**, 5657-5678.
- 256 S. Schlienger, J. Alauzun, F. Michaux, L. Vidal, J. Parmentier, C. Gervais, et al., *Chem. Mater.*, 2012, **24**, 88-96.
- 257 B. Hosseini, A. A. Nourbakhsh and K. J. D. MacKenzie, *Ceram. Int.*, 2015, **41**, 8809-8813.
- 258 N. D. Shcherban, S. M. Filonenko and P. S. Yaremov, *Theor. Exp. Chem.*, 2017, **52**, 358-363.
- 259 M. P. Suh, H. J. Park, T. K. Prasad and D. W. Lim, *Chem Rev*, 2012, **112**, 782-835.
- 260 Q. Lai, M. Paskevicius, D. A. Sheppard, C. E. Buckley, A. W. Thornton, M. R. Hill, et al., *ChemSusChem*, 2015, **8**, 2789-2825.
- 261 S. Niaz, T. Manzoor and A. H. Pandith, *Renew. Sustain. Energy Rev.*, 2015, **50**, 457-469.
- 262 DOE Targets for Onboard Hydrogen Storage Systems for Light-Duty Vehicles, https://www.energy.gov/sites/prod/files/2017/05/f34/fcto_myredd_table_onboard_h2_storage_systems_doe_targets_ldv_1.pdf (last accessed April 2018).
- 263 W. C. Conner and J. L. Falconer, *Chem. Rev.*, 1995, **95**, 759-788.
- 264 R. Prins, *Chem. Rev.*, 2012, **112**, 2714-2738.
- 265 H. Nishihara, T. Simura and T. Kyotani, *Chem. Commun.*, 2018, **54**, 3327-3330.
- 266 J. P. Marco-Lozar, M. Kunowsky, F. Suarez-Garcia, J. D. Carruthers and A. Linares-Solano, *Energy Environ. Sci.*, 2012, **5**, 9833-9842.
- 267 K. Sumida, M. R. Hill, S. Horike, A. Dailly and J. R. Long, *J. Am. Chem. Soc.*, 2009, **131**, 15120-15121.
- 268 D. Yuan, D. Zhao, D. Sun and H. C. Zhou, *Angew. Chem. Int. Ed.*, 2010, **49**, 5357-5361.
- 269 T. A. Makal, J. R. Li, W. Lu and H. C. Zhou, *Chem. Soc. Rev.*, 2012, **41**, 7761-7779.
- 270 S. Gadipelli and Z. X. Guo, *Prog. Mater. Sci.*, 2015, **69**, 1-60.
- 271 P. Silva, S. M. F. Vilela, J. P. C. Tome and F. A. Almeida Paz, *Chem. Soc. Rev.*, 2015, **44**, 6774-6803.
- 272 Y. Cui, B. Li, H. He, W. Zhou, B. Chen and G. Qian, *Acc. Chem. Res.*, 2016, **49**, 483-493.
- 273 C. M. Simon, J. Kim, D. A. Gomez-Gualdrón, J. S. Camp, Y. G. Chung, R. L. Martin, et al., *Energy Environ. Sci.*, 2015, **8**, 1190-1199.
- 274 Y. Peng, V. Krungleviciute, I. Eryazici, J. T. Hupp, O. K. Farha and T. Yildirim, *J. Am. Chem. Soc.*, 2013, **135**, 11887-11894.
- 275 F. Gándara, H. Furukawa, S. Lee and O. M. Yaghi, *J. Am. Chem. Soc.*, 2014, **136**, 5271-5274.
- 276 B. Li, H. M. Wen, H. Wang, H. Wu, M. Tyagi, T. Yildirim, et al., *J. Am. Chem. Soc.*, 2014, **136**, 6207-6210.
- 277 J. A. Mason, M. Veenstra and J. R. Long, *Chem. Sci.*, 2014, **5**, 32-51.
- 278 K. Sumida, D. L. Rogow, J. A. Mason, T. M. McDonald, E. D. Bloch, Z. R. Herm, et al., *Chem. Rev.*, 2012, **112**, 724-781.
- 279 Y. Belmabkhout, V. Guillerm and M. Eddaoudi, *Chem. Eng. J.*, 2016, **296**, 386-397.
- 280 H. A. Patel, J. Byun and C. T. Yavuz, *ChemSusChem*, 2017, **10**, 1303-1317.
- 281 M. Sevilla and A. B. Fuertes, *Energy Environ. Sci.*, 2011, **4**, 1765-1771.
- 282 H. Furukawa, N. Ko, Y. B. Go, N. Aratani, S. B. Choi, E. Choi, et al., *Science*, 2010, **329**, 424-428.
- 283 J. A. Mason, K. Sumida, Z. R. Herm, R. Krishna and J. R. Long, *Energy Environ. Sci.*, 2011, **4**, 3030-3040.
- 284 T. M. McDonald, D. M. D'Alessandro, R. Krishna and J. R. Long, *Chem. Sci.*, 2011, **2**, 2022-2028.
- 285 R. Kotz and M. Carlen, *Electrochim. Acta*, 2000, **45**, 2483-2498.
- 286 P. Simon and Y. Gogotsi, *Nat. Mater.*, 2008, **7**, 845-854.
- 287 G. Wang, L. Zhang and J. Zhang, *Chem. Soc. Rev.*, 2012, **41**, 797-828.
- 288 S. Iwamura, H. Nishihara and T. Kyotani, *J. Phys. Chem. C*, 2012, **116**, 6004-6011.
- 289 M. Gauthier, D. Mazouzi, D. Reyter, B. Lestriez, P. Moreau, D. Guyomard, et al., *Energy Environ. Sci.*, 2013, **6**, 2145.
- 290 S. Iwamura, H. Nishihara and T. Kyotani, *J. Power Sources*, 2013, **222**, 400-409.
- 291 T. Kasukabe, H. Nishihara, K. Kimura, T. Matsumoto, H. Kobayashi, M. Okai, et al., *Sci. Rep.*, 2017, **7**, 42734.